

The Irregular Satellites of Saturn

Tilmann Denk

Freie Universität Berlin

Stefano Mottola

Deutsches Zentrum für Luft- und Raumfahrt

Federico Tosi

Istituto di Astrofisica e Planetologia Spaziali

William F. Bottke

Southwest Research Institute

Douglas P. Hamilton

University of Maryland, College Park

With 38 known members, the outer or irregular moons constitute the largest group of satellites in the saturnian system. All but exceptionally big Phoebe were discovered between the years 2000 and 2007. Observations from the ground and from near-Earth space constrained the orbits and revealed their approximate sizes (~4 to ~40 km), low visible albedos (likely below ~0.1), and large variety of colors (slightly bluish to medium-reddish). These findings suggest the existence of satellite dynamical families, indicative of collisional evolution and common progenitors. Observations with the Cassini spacecraft allowed lightcurves to be obtained that helped determine rotational periods, coarse shape models, pole-axis orientations, possible global color variations over their surfaces, and other basic properties of the irregulars. Among the 25 measured moons, the fastest period is 5.45 h. This is much slower than the disruption rotation barrier of asteroids, indicating that the outer moons may have rather low densities, possibly as low as comets. Likely non-random correlations were found between the ranges to Saturn, orbit directions, object sizes, and rotation periods. While the orbit stability is higher for retrograde objects than for progrades very far away from Saturn, a compelling physical cause for size and spin relations to orbital elements is not yet known. The large moon Phoebe was resolved by Cassini during a close flyby in June 2004, showing numerous craters of all sizes on a surface composed of water ice and amorphous carbon. While the origin of the irregulars is still debated, capture of comets via three-body interactions during giant planet encounters do the best job thus far at reproducing the observed orbits. This chapter gives a summary of our knowledge of Saturn’s irregular moons as of the end of 2017.

1. INTRODUCTION

The outer or irregular moons of Saturn are a class of objects that is very distinct from the other satellites treated in this book. It not only has more objects (38 are presently known) than the class of the inner moons (24), but also occupies a much larger volume within the Hill sphere of Saturn. On the other hand, almost all “irregulars” are quite small: Besides the large moon Phoebe (213 km diameter), 37 objects of sizes on the order of ~40 km down to ~4 km are known (the uncertainties of the diameter values are still substantial). Additional ones smaller than 4 km certainly

exist as well. Therefore, they significantly contribute to the total number, but not to the overall mass of Saturn’s satellite system (less than 0.01%).

The discrimination between regular (or inner) and irregular (or outer) satellites is through distance to the center planet, orbit eccentricities, and inclinations. The irregulars reach ranges to Saturn between 7.6×10^6 km (at the perapsis of Kiviuq; ~12% of Saturn’s Hill sphere radius of $\sim 65 \times 10^6$ km) and 33×10^6 km (~50% of the Hill radius at the apoapsis of Surtur). They require between 1.3 and 4.1 years (Ijiraq and Fornjot, respectively) for one revolution around Saturn. As a comparison, Iapetus, the regular

satellite farthest from Saturn, has an apoapsis distance of 3.6×10^6 km and requires just 0.22 years for one orbit. The separation distance is the so-called critical semimajor axis (Goldreich, 1966; Burns, 1986), which depends on the mass and radius of Saturn, the quadrupole gravitational harmonic J_2' of the saturnian system (e.g., Tremaine *et al.*, 2009), as well as the distance Saturn-to-Sun and the mass of the Sun. This range marks the location where the precession of the satellite's orbital plane is dominated by the Sun rather than by the planet's oblateness (e.g., Shen and Tremaine, 2008). For Saturn, $a_{\text{crit}} \sim 3.4 \times 10^6$ km or ~5% of its Hill sphere; this is close to the orbit of Iapetus (which is not considered as an irregular moon although many mysteries about its origin still exist). The orbit eccentricities of Saturn's irregulars vary between 0.11 and 0.54, while the orbits of the regular moons, except for Hyperion, are almost circular ($e < 0.03$). The inclinations of the regular moons against the local Laplace plane are very close to zero (Iapetus with $i \sim 8^\circ$ deviates most), while those of the irregulars may by principle vary between 0° and 180° , indicating that they might reside on retrograde paths (planetocentric coordinate system). At Saturn, 9 prograde and 29 retrograde irregular moons have been discovered so far. All were found in the stable dynamical region that surrounds Saturn (Carruba *et al.*, 2002; Nesvorný *et al.*, 2003; Shen and Tremaine, 2008).

As with all satellites of Saturn, the irregular moons cannot be seen by the naked eye. Therefore, the irregulars were unknown to the ancients, and Phoebe was discovered only 119 years before the publication of this book (Pickering, 1899a,b). Nevertheless, its discovery contained several "firsts": Phoebe was not just the first saturnian irregular moon to be discovered, but also the first outer (far distant) moon of any planet. It was the first-ever discovery of a moon through photography and the first moon in the solar system of which the direction of motion is opposite to the other moons of the common planet (Pickering, 1905).

The other irregulars of Saturn are even much fainter than Phoebe. Siarnaq and Albiorix barely scratch the 20-mag mark (V-band magnitude), and the others do not exceed 21 to 25 mag even under ideal observation conditions, making them difficult targets for Earth-based observers. An additional issue for observing these objects from Earth is the proximity of the very bright planet. For example, an orbital radius of 13×10^6 km translates into a maximum elongation of 30' from Saturn, which becomes a challenge — especially for small objects — due to the planet's straylight. All the other 37 irregular moons of Saturn were thus discovered rather recently (Table 1). Their discovery became possible with the introduction of highly sensitive large CCDs in combination with very large telescopes and the ability to process large volumes of data (Gladman *et al.*, 1998, 2001; Nicholson *et al.*, 2008). Furthermore, the impending arrival of the Cassini spacecraft was a major driver for the initiation of this search.

Saturn is not the only home of irregular satellites. All four large planets of our solar system host a large number of outer moons that revolve around their planet at large distances of

many million kilometers on eccentric and inclined orbits. Similarly to the Jupiter Trojan asteroids, comets, Centaurs, Plutinos, classical Kuiper belt objects, etc., they constitute a distinct group of numerous objects residing in the outer solar system. As of the end of 2017, 114 outer moons were known in the solar system. Sixty-one of these moons orbit Jupiter, 38 orbit Saturn, 9 orbit Uranus, and 6 orbit Neptune. Most of them (96) were discovered between 10 and 20 years before the publication of this book, all through direct imaging from Earth. Before 1998, just 12 outer moons were known: Phoebe, Neptune's Nereid (discovered in 1949), the two uranian moons Sycorax and Caliban (discovered in 1997), and the eight "classical" irregulars of Jupiter (discovered between 1904 and 1974). A comprehensive summary of the different systems of irregular satellites is provided in Nicholson *et al.* (2008). Other nice summaries were written by Sheppard (2006), Jewitt *et al.* (2006), and Jewitt and Haghighipour (2007).

After the decade of extensive discoveries, almost no additional objects have been reported. The reason is presumably that few are left undiscovered at the accessible brightness ranges (e.g., Hamilton, 2001), but also that the required large telescopes are highly contested. Besides providing our summary of the state of the knowledge of the saturnian irregular moons, one task of this chapter is thus to motivate and encourage a new generation of solar system astronomers to initiate new search programs to discover the still fainter irregular moons and to help to further complete their inventory.

Ironically, the satellite discovery boom of the first decade of this century allowed the irregular moons to outnumber the regular planetary moons. While the ratio between inner and outer satellites of the giant planets was 48:11 in 1996, it is now 58:114. Thus, "irregular" is the rule, and "regular" the minority, at least by number of objects. However, outrivalling both groups are the known or suspected moons of the minor bodies. As of April 2018, 348 potential companions of 331 asteroids and transneptunian objects (TNOs) were listed (Johnston, 2018).

What do we know about the irregular moons of Saturn, and how did we learn it? What we know quite well for a large majority of them are astronomical properties like the orbital elements that were determined from Earth and for which a brief description is given in section 2.1. Roughly known or estimated are physical properties like absolute magnitudes, albedos (and combined the approximate sizes), or colors for the brightest objects. This knowledge comes from photometric measurements of groundbased observation data and from the Spitzer and Near-Earth Object Wide-field Infrared Survey Explorer (NEOWISE) missions and is presented in section 2.2. An important tool to obtain physical information, especially many rotational periods, was Cassini's Imaging Science Subsystem (ISS) (Porco *et al.*, 2004). Although operating at Saturn, Cassini was still too far away from the irregulars to resolve their surfaces (except for Phoebe). Section 3, which is mainly based on the work of Denk and Mottola (in preparation, 2018, hereafter DM18), summarizes some of the Cassini-based ongoing research of

Saturn's irregulars. Phoebe, discussed in section 4, was the sole irregular moon of Saturn where disk-resolved images of the surface were obtained by Cassini, mainly during the close flyby. The origin of the irregular moons is still debated.

Several mechanisms were proposed, and the status quo is briefly described in section 5. The chapter ends with a summary of the most important missing information as well as prospects for future exploration (section 6).

TABLE 1. Discovery circumstances of Saturn's 38 irregular moons.

Moon Name	IAU Number	Provisional Designation	SPICE ID*	Observation Date†	Discoverer Group‡	IAU Circ. No.	IAU Circ. Issued§	Moon Abbrev.¶
Phoebe	IX	—	609	16 Aug 1898	Pickering	—	17 Mar 1899	Pho
Ymir	XIX	S/2000 S 1	619	07 Aug 2000	Gladman	7512	25 Oct 2000	Ymi
Paaliaq	XX	S/2000 S 2	620	07 Aug 2000	Gladman	7512	25 Oct 2000	Paa
Siarnaq	XXIX	S/2000 S 3	629	23 Sep 2000	Gladman	7513	25 Oct 2000	Sia
Tarvos	XXI	S/2000 S 4	621	23 Sep 2000	Gladman	7513	25 Oct 2000	Tar
Kiviuq	XXIV	S/2000 S 5	624	07 Aug 2000	Gladman	7521	18 Nov 2000	Kiv
Ijiraq	XXII	S/2000 S 6	622	23 Sep 2000	Gladman	7521	18 Nov 2000	Iji
Thrymr	XXX	S/2000 S 7	630	23 Sep 2000	Gladman	7538	07 Dec 2000	Thr
Skathi	XXVII	S/2000 S 8	627	23 Sep 2000	Gladman	7538	07 Dec 2000	Ska
Mundilfari	XXV	S/2000 S 9	625	23 Sep 2000	Gladman	7538	07 Dec 2000	Mun
Erriapus	XXVIII	S/2000 S 10	628	23 Sep 2000	Gladman	7539	07 Dec 2000	Err
Albiorix	XXVI	S/2000 S 11	626	09 Nov 2000	Holman	7545	19 Dec 2000	Alb
Suttungr	XXIII	S/2000 S 12	623	23 Sep 2000	Gladman	7548	23 Dec 2000	Sut
Narvi	XXXI	S/2003 S 1	631	08 Apr 2003	Sheppard	8116	11 Apr 2003	Nar
S/2004 S 7		S/2004 S 7	65035	12 Dec 2004	Jewitt	8523	04 May 2005	4S7
Fornjot	XLII	S/2004 S 8	642	12 Dec 2004	Jewitt	8523	04 May 2005	For
Farbauti	XL	S/2004 S 9	640	12 Dec 2004	Jewitt	8523	04 May 2005	Far
Aegir	XXXVI	S/2004 S 10	636	12 Dec 2004	Jewitt	8523	04 May 2005	Aeg
Bebhionn	XXXVII	S/2004 S 11	637	12 Dec 2004	Jewitt	8523	04 May 2005	Beb
S/2004 S 12		S/2004 S 12	65040	12 Dec 2004	Jewitt	8523	04 May 2005	4S12
S/2004 S 13		S/2004 S 13	65041	12 Dec 2004	Jewitt	8523	04 May 2005	4S13
Hati	XLIII	S/2004 S 14	643	12 Dec 2004	Jewitt	8523	04 May 2005	Hat
Bergelmir	XXXVIII	S/2004 S 15	638	12 Dec 2004	Jewitt	8523	04 May 2005	Ber
Fenrir	XLI	S/2004 S 16	641	13 Dec 2004	Jewitt	8523	04 May 2005	Fen
S/2004 S 17		S/2004 S 17	65045	13 Dec 2004	Jewitt	8523	04 May 2005	4S17
Bestla	XXXIX	S/2004 S 18	639	13 Dec 2004	Jewitt	8523	04 May 2005	Bes
Hyrrokkin	XLIV	S/2004 S 19	644	12 Dec 2004	Sheppard	8727	30 Jun 2006	Hyr
S/2006 S 1		S/2006 S 1	65048	04 Jan 2006	Sheppard	8727	30 Jun 2006	6S1
Kari	XLV	S/2006 S 2	645	04 Jan 2006	Sheppard	8727	30 Jun 2006	Kar
S/2006 S 3		S/2006 S 3	65050	05 Jan 2006	Sheppard	8727	30 Jun 2006	6S3
Greip	LI	S/2006 S 4	651	05 Jan 2006	Sheppard	8727	30 Jun 2006	Gre
Loge	XLVI	S/2006 S 5	646	05 Jan 2006	Sheppard	8727	30 Jun 2006	Log
Jarnsaxa	L	S/2006 S 6	650	05 Jan 2006	Sheppard	8727	30 Jun 2006	Jar
Surtur	XLVIII	S/2006 S 7	648	05 Jan 2006	Sheppard	8727	30 Jun 2006	Sur
Skoll	XLVII	S/2006 S 8	647	05 Jan 2006	Sheppard	8727	30 Jun 2006	Sko
Tarqeq	LII	S/2007 S 1	652	16 Jan 2007	Sheppard	8836	11 May 2007	Taq
S/2007 S 2		S/2007 S 2	65055	18 Jan 2007	Sheppard	8836	11 May 2007	7S2
S/2007 S 3		S/2007 S 3	65056	18 Jan 2007	Sheppard	8836	11 May 2007	7S3

* For SPICE, see JPL's NAIF web page (<https://naif.jpl.nasa.gov/>).

† Object was first spotted in an image taken on that date. Some of the 2006 objects were later found in 2004 data as well.

‡ The discoverer groups included the following: 1899: W. H. Pickering, Stewart; 2000: Gladman, Kavelaars, Petit, Scholl, Holman, Marsden, Nicholson, Burns; 2003: Sheppard; 2005, 2006, 2007: Sheppard, Jewitt, Kleyna.

§ Day of official announcement of the discovery. Phoebe was announced in a handwritten Bulletin of the Harvard College Observatory (Pickering, 1899a; the first IAU circular was published no earlier than October 1922).

¶ Abbreviations of moon names used in the figures.

2. RESULTS FROM (NEAR) EARTH OBSERVATIONS

2.1. Orbital Properties

Figure 1, based on the numbers of Table 2, shows the “orbital architecture” of the irregular-moon system of Saturn. The mean orbital elements a and i are displayed in a polar-coordinate plot, with the apoapsis-periapsis excursion being shown as thin bars for each object as a proxy for the eccentricity e . The inclinations are measured against the local Laplace plane, which is very close to the orbit plane of Saturn about the Sun for all irregulars. From Fig. 1, it becomes obvious that a fundamental classification of the irregular moons is the discrimination into objects with prograde and retrograde motions about Saturn in planetocentric coordinates. Furthermore, many of the moons cluster around similar a - e - i values and are thus likely parts of a “family” or the partners of a “pair.” Possible relations are marked in Fig. 1 and Table 2.

Members of an object family share similar orbital elements and are genetically related, but not gravitationally bound anymore to each other. Among asteroids, families are believed to have formed through catastrophic collisions (e.g., Margot *et al.*, 2015). On the other hand, a pair contains just two objects that originally co-orbited, but for whatever reason separated in the past. Among Saturn’s irregular moons, there are several objects that share their orbital elements with just one other moon. In this chapter, we will use the term “pair” for them although their origin is not known. They might be true orbital pairs, but also of collisional origin from a single object where smaller family members were simply not yet discovered. The existence of families

among Saturn’s irregulars was suspected soon after the first discoveries were made (Gladman *et al.*, 2001; Grav *et al.*, 2003). Their presence indicates that the individual irregulars we observe today might not have been captured independently, but could be remnants of originally larger moons.

Among the prograde objects, there exist two distinct inclination groups. The Gallic group (Albiorix, Tarvos, Enriapus, and Bebhionn, named after Gallic mythology characters) [for satellite naming, see, e.g., Blunck (2010)] is well clustered in the a - e - i space (Fig. 1, Table 2) and thus likely represents a collisional family; Turrini *et al.* (2008) modeled a dispersion velocity of $\sim 130 \text{ m s}^{-1}$. For the other five prograde moons (Siarnaq, Paaliaq, Kiviuq, Ijiraq, Tarqeeq), dubbed the Inuit group (named after characters from the Inuit folklore and mythology), a common origin is rather questionable. They share an inclination value of $i \sim 46^\circ$, but their semimajor axes ($a \sim 11.4$ to $18.2 \times 10^6 \text{ km}$) and eccentricities ($e \sim 0.17$ to 0.33) are quite different. However, within the Inuit group, Turrini *et al.* (2008) found a dispersion velocity of only $\sim 100 \text{ m s}^{-1}$ for the Ijiraq/Kiviuq satellite pair, making a common progenitor very plausible for these two objects. Siarnaq and Tarqeeq might also form a pair, while no partner is known for Paaliaq.

The mean orbital elements of the 29 known retrograde objects, sometimes called the Norse group, widely range from $a = 12.9$ to $25.2 \times 10^6 \text{ km}$, $e = 0.11$ to 0.52 , and $i = 145^\circ$ to almost 180° . Herein, the orbit of large irregular moon Phoebe is very different from that of all other objects, and a clustering as for the progrades is not immediately obvious. In the work of Turrini *et al.* (2008), only one cluster of seven objects, but otherwise only small groups of two or three moons, show rather moderate dispersion velocities below 170 m s^{-1} . These potential families include only half of the

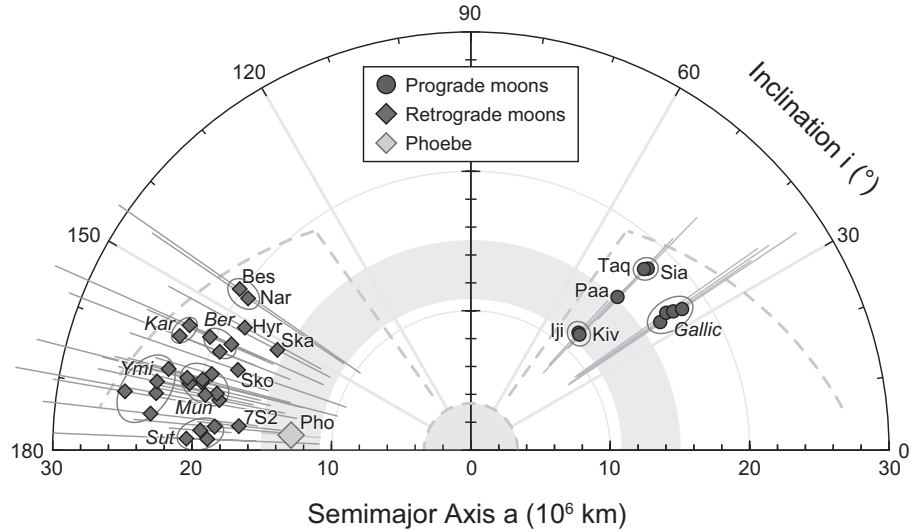


Fig. 1. Polar plot of the a - i space for the 38 irregular moons of Saturn. The thin bars are proxies for the eccentricities, by showing periapsis and apoapsis distances of each object. The light-gray band indicates the sphere of influence of Phoebe. The dashed lines show a_{crit} and apparent outer boundaries of the semimajor axes and inclinations for the irregulars. Most of the potential families or pairs are encircled. Individual moons are labeled except for members of families where only the name of the family is given (according to Table 2).

known retrogrades. In this context, it must be cautioned that some orbital elements used at the time of Turrini's work differed considerably from current, updated values, and that the orbits of six retrogrades are still so poorly determined that they are considered lost [objects S/2006 S 1, S/2004 S 7, S/2004 S 13, S/2007 S 3, S/2007 S 2, and S/2004 S 13

(Jacobson et al., 2012)]. We thus suggest a slightly modified grouping with about half a dozen pairs and families where just 3–6 retrogrades (plus potentially Phoebe) were left as stand-alone moons (Fig. 1, Table 2).

A noticeable difference between the prograde and the retrograde moons are their average distances to Saturn. The

TABLE 2. Astronomical properties and sizes of Saturn's 38 irregular moons.

Moon Name	Group Member	Family/ Pair*	\times^{\dagger}	a (10^6 km) ‡	e ‡	i ($^{\circ}$) ‡	i' ($^{\circ}$) ‡	P (a) ‡	H (mag) $^{\$}$	App. Mag. $^{\ \hspace{-0.1cm}\ }$	Size (km) **	Moon Abbrev.
Phoebe	retro	?	—	12.95	0.16	175.2	4.8	1.50	6.6	16	213	Pho
Kiviuq	Inuit	(Iji)	×	11.38	0.33	46.8	46.8	1.23	12.6	22.0	17	Kiv
Ijiraq	Inuit	(Kiv)	×	11.41	0.27	47.5	47.5	1.24	13.2	22.6	13	Iji
Paaliaq	Inuit	—	×	15.20	0.33	46.2	46.2	1.88	11.7	21.3	25	Paa
Tarqeeq	Inuit	(Sia)	×	17.96	0.17	46.3	46.3	2.43	14.8	23.9	6	Taq
Siarnaq	Inuit	(Taq)	×	18.18	0.28	45.8	45.8	2.45	10.6	20.1	42	Sia
Albiorix	Gallic	Gallic	×	16.39	0.48	34.1	34.1	2.15	11.1	20.5	33	Alb
Bebhionn	Gallic	Gallic	×	17.12	0.47	35.1	35.1	2.29	15.0	24.1	6	Beb
Erriapus	Gallic	Gallic	×	17.60	0.47	34.5	34.5	2.38	13.7	23.0	10	Err
Tarvos	Gallic	Gallic	×	18.24	0.54	33.7	33.7	2.53	12.9	22.1	15	Tar
Narvi	retro	(Bes)	×	19.35	0.43	145.7	34.3	2.75	14.4	23.8	7	Nar
Bestla	retro	(Nar)	×	20.21	0.51	145.1	34.9	2.98	14.6	23.8	7	Bes
Skathi	retro	—	×	15.64	0.27	152.6	27.4	1.99	14.3	23.6	8	Ska
S/2007 S 2	retro	—	×	16.7	0.18	174	6	2.21	15.3	24.4	5	7S2
Skoll	retro	—	×	17.67	0.46	161.0	19.0	2.40	15.4	24.5	5	Sko
Hyrrokkin	retro	(Gre?)	×	18.44	0.34	151.5	28.5	2.55	14.3	23.5	8	Hyr
Greip	retro	Sut? (Hyr?)	×	18.46	0.32	174.8	5.2	2.56	15.4	24.4	5	Gre
S/2007 S 3	retro	Sut		18.9	0.19	178	2	2.68	15.8	24.9	4	7S3
Suttungr	retro	Sut		19.47	0.11	175.8	4.2	2.78	14.5	23.9	7	Sut
Thrymr	retro	Sut? (4S7?)	×	20.42	0.47	177.7	2.3	3.00	14.3	23.9	8	Thr
S/2004 S 13	retro	Mun	×	18.4	0.26	169	11	2.56	15.6	24.5	4	4S13
Mundilfari	retro	Mun	×	18.65	0.21	167.4	12.6	2.61	14.5	23.8	7	Mun
Jarnsaxa	retro	Mun		19.35	0.22	163.6	16.4	2.76	15.6	24.7	4	Jar
S/2004 S 17	retro	Mun		19.4	0.18	168	12	2.78	16.0	25.2	4	4S17
Hati	retro	Mun	×	19.87	0.37	165.8	14.2	2.99	15.3	24.4	5	Hat
S/2004 S 12	retro	Mun	×	19.89	0.33	165.3	14.7	2.86	15.7	24.8	4	4S12
Aegir	retro	Mun		20.75	0.25	166.7	13.3	3.06	15.5	24.4	4	Aeg
S/2004 S 7	retro	Mun? (Thr?)	×	21.0	0.53	166	14	3.12	15.2	24.5	5	4S7
S/2006 S 1	retro	Ber		18.8	0.14	156	24	2.64	15.5	24.6	4	6S1
Bergelmir	retro	Ber		19.34	0.14	158.6	21.4	2.75	15.2	24.2	5	Ber
Farbauti	retro	Ber (?)		20.39	0.24	156.5	23.5	2.98	15.7	24.7	4	Far
Kari	retro	Kar	×	22.09	0.48	156.1	23.9	3.37	14.8	23.9	6	Kar
S/2006 S 3	retro	Kar	×	22.43	0.38	158.6	21.4	3.36	15.6	24.6	4	6S3
Fenrir	retro	Ymi		22.45	0.13	165.0	15.0	3.45	15.9	25.0	4	Fen
Surtur	retro	Ymi	×	22.94	0.45	169.7	10.3	3.55	15.8	24.8	4	Sur
Loge	retro	Ymi		23.06	0.19	167.7	12.3	3.59	15.3	24.6	5	Log
Ymir	retro	Ymi		23.13	0.33	173.5	6.5	3.60	12.3	21.7	19	Ymi
Fornjot	retro	Ymi		25.15	0.21	170.4	9.6	4.09	14.9	24.6	6	For

* Suggestions according to Fig. 1 (see also text). For just two objects, the partner is given in parentheses.

[†] Checked if periaxis range of moon is smaller than apoaosis range of Phoebe.

[‡] Orbital semimajor axis a, eccentricity e, inclination i, inclination supplemental angle $i' = 90^{\circ} - |90^{\circ} - i|$, orbit period P. Planetocentric coordinates; from JPL's solar-system dynamics website (<https://ssd.jpl.nasa.gov/>).

[§] Absolute magnitude H; the numbers may be uncertain by several tenths of magnitude. From MPC ephemeris service (<http://www.minorplanetcenter.net/iau/NatSats/NaturalSatellites.html>).

[¶] Apparent optical magnitude (R-band) from Earth; from S. Sheppard's satellite and moon web page (<https://home.dtm.ciw.edu/users/sheppard/satellites/>).

^{**} Calculated from H and assumed albedo A = 0.06 through D = $2 \times 1 \text{ au} \times A^{-0.5} \times 10^{-0.2(H-M_{\odot})}$; with $M_{\odot} = -26.71 \pm 0.02 \text{ mag}$ (Pecaut and Mamajek, 2013). Note that the errors may be large. Phoebe's value is from Castillo-Rogez et al. (2012).

average semimajor axis of the progrades is $\sim 16 \times 10^6$ km and thus clearly smaller than the $\sim 20 \times 10^6$ km for the retrogrades. That more “space” is used by retrograde objects appears to be a common phenomenon among the irregular-moon systems of all four giant planets (e.g., Carruba *et al.*, 2002; Nicholson *et al.*, 2008; work on this issue goes back to Hénon, 1969). Orbital stability curves in Nesvorný *et al.* (2003) (see also Shen and Tremaine, 2008) show a distinct asymmetry between prograde and retrograde, which they interpret as being due to the asymmetric location of a phenomenon called the ejection resonance. In addition, the curved dashed line in Fig. 1 indicates that objects with inclinations near 180° , i.e., close to Saturn’s orbit plane, may have larger semimajor axes than objects on highly tilted orbits. Approximate inclination limits for long-term stable orbits (Shen and Tremaine, 2008) are also shown in Fig. 1 by straight dashed lines.

The lack of orbits with inclinations $\sim 55^\circ < i < \sim 125^\circ$ is likely a consequence of the Lidov-Kozai effect (Carruba *et al.*, 2002; Nesvorný *et al.*, 2003) where solar perturbations cause oscillations of the inclination and eccentricity. Originally extremely inclined orbits become unstable because the Lidov-Kozai oscillation makes the eccentricity so high that these irregulars reach the inner moon systems or even Saturn itself with the consequence of removal from the system through scattering or collision, or, near apoapsis, reach the edge of the Hill sphere and may escape. Such an inclination gap is found in all irregular-moon systems of the giant planets (Nicholson *et al.*, 2008) (see also section 5). Interestingly, there is also a gap at $0^\circ < i < \sim 25^\circ$, for which the reason is not yet known. This gap is very obvious in the a,e,i-plot in Plate 8 of Nicholson *et al.* (2008); the sole exception is Neptune’s Nereid. However, Nereid is very unusual since it contains approximately twice the mass of all other outer moons of the giant planets combined. It might even not be a captured object, but a former regular moon. Goldreich *et al.* (1989) and Cuk and Gladman (2005) hypothesized in this direction, while Nogueira *et al.* (2011) provided arguments why Nereid could never have been a regular satellite.

A major player in at least the inner parts of Saturn’s irregular-moon system appears to be the dominating moon Phoebe. In a sense behaving like a major planet, Phoebe with its periapsis-to-apoapsis range from 10.8 to 15.1×10^6 km (Fig. 1) partially cleared its surroundings. The semimajor axes for all but two irregulars are actually farther away at 15.2 to 25.2×10^6 km (Table 2), indicating that they are outside the realm of Phoebe for most of the time. Since gravitational scattering among Saturn’s irregulars should be negligible even for close encounters with Phoebe, this “sweeping effect” is likely due to the much larger size of Phoebe and thus its much larger collisional cross-section. Nesvorný *et al.* (2003) calculated mutual collision rates between the 13 individual irregulars known at that time. While for all combinations not including Phoebe, the collision rate per 4.5 Ga is 0.02 or less, for all objects with orbits potentially crossing Phoebe’s orbit it is ≥ 0.2 . For Kiviuq, Ijiraq, and Thrymr, this collision rate is even > 1 , indicating that these moons will likely not survive another 4.5 b.y. From Fig. 1,

it is obvious why these moons are in particular danger of collision with Phoebe: Ijiraq and Kiviuq reside within the ranges of Phoebe for most of the time, thus it is just a question of time as to when one of these moons will pass within ~ 110 km of Phoebe. For Thrymr, the low tilt compared to Phoebe’s orbit lengthens the “corridor” where a collision might take place during the epochs where nodes of the two moons are very close to each other. Among the objects that were not yet known to Nesvorný *et al.* (2003), relatively-low-tilt objects Greip and S/2007 S 2 should be in high danger of eventually colliding with Phoebe as well. Table 2 marks all objects with current periapses lower than Phoebe’s apoapsis as a first-order criterion for “being in danger of collision with Phoebe.” Actually, two-thirds of the known irregulars of Saturn qualify as future Phoebe impactors.

2.2. Physical Properties

Besides orbital properties, groundbased observations and observations from Infrared telescopes close to Earth also revealed fundamental physical properties like approximate sizes, albedos, and colors. The first photometric survey from Grav *et al.* (2003) obtained BVRI (blue, visual, red, infrared) photometry of three Gallic moons (Albiorix, Tarvos, Erriapus), three Inuits (Siarnaq, Paaliaq, Kiviuq), and two retrograde moons (Phoebe, Ymir). The colors were found to vary between “neutral/gray” and “light red”; the asteroidal analogs are C-type and P-/D-type. One rationale behind this research was the hypothesis that objects from similar dynamical families should exhibit the same color if the progenitor object was not differentiated. Grav *et al.* (2003) found the observed Gallic moons in good “color agreement” to each other, and the same for the Inuits. Only Phoebe and Ymir were found to be significantly differently colored, from which they concluded that Ymir should not have been a part of Phoebe in the past.

Through JHK (near-infrared) photometry, Grav and Holman (2004) extended the measurements of Phoebe, Siarnaq, Albiorix, and Paaliaq into the near-infrared. Their seven-color spectra were again consistent with C-, P-, or D-type objects. In this context, it must be cautioned that the use of the terms “C, P, or D type” refers to a color classification originally introduced in the context of asteroids, but that its usage for the irregulars does not necessarily imply that these moons are asteroids that originated in the asteroid belt, nor that they have the same surface composition as asteroids. The terminology for transneptunian objects (TNOs) or Centaurs includes “neutral/gray,” “red,” or “ultra-red” and also simply describes the spectral slopes of the irregulars, but again not the origin region and object type (Grav *et al.*, 2015).

In January 2005, the Saturn opposition led to unusually low phase angles for the irregular moons, with the lowest value of 0.01° reached for Ymir, and 0.03° to 0.11° for six other objects (Bauer *et al.*, 2006). During the same apparition, Miller *et al.* (2011) observed Phoebe’s opposition surge in four color filters. Tarvos and Albiorix, the two Gallic moons, again showed a common behavior, but their phase

curves near 0° were much shallower than for Paaliaq, Ijiraq, and Phoebe. *Bauer et al.* (2006) proposed that the cause of the subdued opposition surge observed for Tarvos and Albiorix may be a higher compaction state of the surface.

The most extensive study of the saturnian irregulars before Cassini was the “deeper look” published by *Grav and Bauer* (2007) (hereafter referred to as *GB07*). They presented broadband four-color photometry at wavelengths between ~ 420 and ~ 820 nm of the 13 brightest objects. These included 3 of the 4 known Gallic moons (Albiorix, Tarvos, Erriapus), 4 of the 5 Inuits (Siarnaq, Paaliaq, Kiviuq, Ijiraq), and 6 of the 29 retrogrades (Skathi, Mundilfari, Thrymr, Suttungr, Ymir; plus earlier data from Phoebe). The four-point spectra were compared through mean spectral slopes. The goal of the work was again to detect correlations between dynamical families and spectral properties. While the colors and spectral slopes were mostly found to be consistent with C-, P-, and D-type objects, the measured diversity in surface colors was surprising. The spectral slope range was found to vary between ~ -5 and $\sim +20\% /_{100 \text{ nm}}$ (Table 3).

Among the Gallic moons, homogeneous colors were found (slopes $\sim +5\% /_{100 \text{ nm}}$; P-type) except for two of the three Albiorix measurements. *GB07* suggest that the color of this moon varies over the surface. The Inuit moons were also found to be quite homogeneous in color ($\sim +12\% /_{100 \text{ nm}}$; D-type), except for Ijiraq ($\sim +20\% /_{100 \text{ nm}}$; “red”). The spectral slope of Ijiraq is redder than what is known from Jupiter Trojans, Hildas, or main-belt asteroids, possibly suggesting that Ijiraq originated in the realm of the Kuiper belt objects. Puzzling in this context is that the colors of Ijiraq and Kiviuq appear to be very different, while these two moons are the prime example for a dynamical relation (Fig. 1; Table 2). Among the retrogrades, the results for Ymir showed strong variations at short wavelengths between different apparitions, and a large peak-to-peak amplitude of ~ 0.3 mag at very low phase angles. *GB07* attribute these properties to significant surface variegations and an irregular shape. While the latter is well confirmed by Cassini observations, the former is not (see section 3.2). The measured spectral slopes vary between $\sim +6$ and $\sim +8\% /_{100 \text{ nm}}$, putting Ymir at the boundary between P- and D-type. Other retrograde moons investigated by *GB07* are Suttungr and Thrymr, which are possibly members of the same dynamical family. Their colors appear neutral/gray ($\sim -3\% /_{100 \text{ nm}}$; C-type), as does Mundilfari, the object with the “least-reddish” color ($\sim -5\% /_{100 \text{ nm}}$; C-type). Since Phoebe ($-2.5\% /_{100 \text{ nm}}$; C-type) is also gray, *GB07* speculate that Mundilfari might be a piece from Phoebe from a collision with an impact velocity of ~ 5 km s $^{-1}$. If true, this scenario may work for an interplanetary impactor, but is unlikely for a planetocentric one, and must have occurred very likely in the early history of the solar system.

The lack of so-called ultra-red matter (spectral slope $> +25\% /_{100 \text{ nm}}$) among the irregulars (while common among TNOs) is evident and challenges the hypotheses that assume the transneptunian region is the origin area of the irregular moons. *GB07* mention two possible solutions to this apparent contradiction. One is that space weathering closer

to the Sun might fade them, the other that an increased cratering rate in the saturnian environment might make the surfaces less red. Support for the second idea comes from observational and collisional-modeling work of the Trojan asteroids by *Wong and Brown* (2016), who argue that the red and less-red colors are byproducts of the presence or absence of H₂S ice, which is lost from the surfaces during later collisions. Since collisional evolution was so predominant for the irregulars of Saturn (*Bottke et al.*, 2010), few objects would still be expected to be red. A third possibility might be that the irregulars did not form that far out. *GB07* conclude from the high variegation among the irregular moons of Saturn that they might have two distinct origin regions. Some (the grayish ones) might be former main-belt objects, while the others (the reddish ones) might come from the outer solar system. However, they note a caveat for this scenario: Phoebe, a grayish or even slightly bluish object, was proposed by *Johnson and Lunine* (2005) to originate from the transneptunian region. Consequently, a consensus among the scientists on the origin question still lies ahead of us. Additional aspects of this problem concerning orbital dynamics are given in section 5.

The brightest irregular moons of Saturn were also observed with the Spitzer Space Telescope (*Mueller et al.*, 2008) and with NEOWISE (*Grav et al.*, 2015). Spitzer data at 24 μm of the Gallic moons Albiorix, Tarvos, and Erriapus; of the Inuits Siarnaq, Paaliaq, Kiviuq, and Ijiraq; and of retrograde moons Phoebe and Ymir showed that the albedos should be generally low, probably less than 0.1, similar to cometary nuclei, Jupiter Trojans, and TNOs. Thermal data available for three of the moons indicate rather low thermal inertias, suggestive of regolith-covered surfaces (*Mueller et al.*, 2008). NEOWISE data could be extracted for the three largest moons Phoebe (at 3.4, 12, and 24 μm), Siarnaq, and Albiorix (both at 24 μm through the technique of data stacking). Recording of Paaliaq and Tarvos was also attempted, but these two objects were too faint for a signal to be detected. Siarnaq’s size was determined to 39.3 ± 5.9 km for an albedo of 0.050 ± 0.017 at a signal-to-noise ratio (SNR) of ~ 7 . The results given for Albiorix are 28.6 ± 5.4 km, 0.062 ± 0.028 , and SNR ~ 3 (*Grav et al.*, 2015). For Phoebe, the size and albedo determinations were accurate to $\sim 5\%$ and $\sim 20\%$, respectively, to values determined from the Cassini and Voyager spacecraft.

Approximate sizes of all of Saturn’s irregular moons were also determined from groundbased photometry. The first estimates were given in the International Astronomical Union Circulars (IAUCs) and Minor Planet Electronic Circulars (MPECs) issued by the Central Bureau for Astronomical Telegrams of the International Astronomical Union (IAU) and by the IAU Minor Planet Center, respectively (see also Table 1). Since the irregular moons are unresolved in the data, their sizes cannot be measured directly, but can be estimated from their brightness and by assuming their visible albedos. Values calculated for Saturn’s irregular moons are summarized in Table 2. From their survey, *GB07* determined approximate radii for 12 irregulars. Their values for

TABLE 3. Physical properties and Cassini observations of 25 saturnian irregular moons.*

Moon Name	†	Rotational period (h)‡	(a/b) _{min} §	LC¶	Spectral Slope (%) _{100 nm} **		No. of Obs.††	Cassini Imaging Observations		
					(%/100 nm)***	No. of Obs.††		First–Last (mm/yy)††	Best Mag.‡‡	Phase (°)§§
Phoebe	(a)	9.2735 ± 0.0006	1.01	1	-2.5	8	08/04–01/15	5.1	3–162	Pho
Kiviuq	(b)	21.97 ± 0.16	2.32	2	+11.8	24	06/09–08/17	12.0	4–136	Kiv
Ijiraq	(c)	13.03 ± 0.14	1.08	2	+19.5	11	01/11–04/16	11.8	40–104	Iji
Paaliaq	(d)	18.79 ± 0.09	1.05	4	+10.0	12	11/07–01/17	11.2	21–112	Paa
Tarqeeq	(e)	76.13 ± 0.04	1.32	2		10	08/11–01/17	15.0	15–49	Taq
Siarnaq	(f)	10.18785 ± 0.00005	1.17	3	+13.0	8	03/09–02/15	10.8	4–143	Sia
Albiorix	(g)	13.33 ± 0.03	1.34	2,3	+12.5**	13	07/10–01/17	9.5	5–121	Alb
Bebhionn	(h)	16.33 ± 0.03	1.41	2		9	03/10–07/17	14.6	19–79	Beb
Erriapus	(i)	28.15 ± 0.25	1.51	2	+5.1	15	02/10–12/16	13.6	26–116	Err
Tarvos	(j)	10.691 ± 0.001	1.08	2,3	+5.4	9	07/11–10/16	12.8	1–109	Tar
Narvi	(k)	10.21 ± 0.02		3		4	03/13–01/16	15.6	54–80	Nar
Bestla	(l)	14.6238 ± 0.0001	1.47	2		14	10/09–11/15	13.5	30–96	Bes
Skathi	(m)	11.10 ± 0.02	1.27	2	+5.2	8	03/11–08/16	15.1	15–77	Ska
Skoll	(n)	7.26 ± 0.09 (?)	1.14	3		2	11/13–02/16	15.5	42–47	Sko
Hyrrokkin	(o)	12.76 ± 0.03	1.27	3		7	03/13–03/17	14.4	20–82	Hyr
Greip	(p)	12.75 ± 0.35 (?)	1.18	2 (?)		1	09/15	15.4	27	Gre
Suttungr	(q)	7.67 ± 0.02	1.18	2,3	-3.2	5	05/11–11/16	15.4	12–72	Sut
Thrymr	(r)	38.79 ± 0.25 (?)	1.21	2 (?)	-3.0	9	11/11–09/17	14.9	13–105	Thr
Mundilfari	(s)	6.74 ± 0.08	1.43	2	-5.0	1	03/12	15.3	36	Mun
Hati	(t)	5.45 ± 0.04	1.42	2		6	02/13–12/15	15.3	14–73	Hat
Bergelmir	(u)	8.13 ± 0.09	1.13	2		2	10/10–09/15	15.9	16–26	Ber
Kari	(v)	7.70 ± 0.14		3		1	10/10	14.8	56	Kar
Loge	(w)	6.9 ± 0.1 ?	1.04	2 ?		2	10/11–02/15	16.2	12	Log
Ymir	(x)	11.92220 ± 0.00002	1.37	3	+8.1	9	04/08–07/15	13.2	2–102	Ymi
Fornjot	(y)	9.5 ?	1.11	3 ?		2	03/14–04/14	16.4	17–30	For

* Cassini high-level observation descriptions and processed data of irregular moons are provided on T. Denk's "Outer Moons of Saturn" web page (<https://tilmanndenk.de/outersaturnianmoons/>).

† Corresponding character in the itemization in section 3.2.

‡ Rotational periods from DM18 and unpublished data. A question mark indicates that the period is not completely unambiguous. The Phoebe value is from Bauer *et al.* (2004).

§ Minimum ratio of the equatorial axes of a reference ellipsoid of uniform albedo with dimensions a and b (derived from the lightcurve amplitudes). The Phoebe value is from Castillo-Rogez *et al.* (2012).

¶ Amount of maxima and minima in the lightcurves; see text.

** Spectral slope S_2' from Table 3 of GB07. Positive values indicate reddish, negative bluish spectra. GB07 give errors between ±0.3 and ±2.8%_{100 nm}. Individual measurements for Albiorix (+5.3, +12.9, +14.9%_{100 nm}) vary much more.

†† Number of Cassini imaging observation "requests" ("visits") where data of the object were achieved. The targeted flyby of Phoebe (June 2004) and data from optical navigation are not included in the counts.

‡‡ Best magnitude of the object as seen from Cassini at a time where data were acquired.

§§ Lowest and highest observation phase angles during Cassini observations. Phase angles from Earth are always <7°.

the absolute magnitude H are systematically higher by ~0.2 to ~0.6 mag compared to the values from the Minor Planet Center. However, for consistency throughout all 38 objects, we use the values of the Minor Planet Center in Table 2, but with the albedos set to 0.06 for the diameter calculations to stay close to the diameter values by GB07, who assumed albedos of 0.08. An assumed albedo of 0.06 is also consistent with the NEOWISE measurements of Albiorix and Siarnaq

described above, for which the determined diameters are within the error bars of the NEOWISE results and of Table 2. These numbers imply that 7 of the 9 known progrades should be between ~10 and ~40 (maybe up to ~50) km in size, while only 2 of 29 retrograde moons are larger than 10 km (Phoebe and Ymir).

With respect to the rotational periods, very little work from the ground has been published. For the relatively

bright object Phoebe, the spin rate has been known for a long time. It was first determined through data from Voyager 2 from *Thomas et al.* (1983) to 9.4 ± 0.2 h, a few years later from Earth by *Kruse et al.* (1986) to 9.282 ± 0.015 h, and eventually more accurately by *Bauer et al.* (2004) to 9.2735 ± 0.0006 h. For the other saturnian irregulars, only fragmentary lightcurve observations of Siarnaq (*Buratti et al.*, 2005; *Bauer et al.*, 2006) and Ymir (*GB07*) indicated perceptible amplitudes, but no reliable periods were given.

3. CASSINI RESEARCH

3.1. Observing Irregular Moons with Cassini

With the Cassini spacecraft en route to Saturn and then orbiting the planet during and after the time of the discovery of the irregular-moon system, a set of small telescopes and spectrometers was well placed close to the irregular moons for many years. Among these instruments, the Narrow Angle Camera (NAC) of the ISS experiment (*Porco et al.*, 2004) was best suited to perform the task of recording these objects. Except during the first orbit, Cassini was rarely more than $\sim 4 \times 10^6$ km away from Saturn, and most of the time even closer than $\sim 2 \times 10^6$ km and thus always inside the orbits of the irregulars. One consequence of this inside location of Cassini was that a dedicated irregular-moon search was not promising because the area to consider filled half the sky.

Observations were performed between ~ 43 and ~ 275 times closer to the irregular saturnian moons than Earth. The closest range to an irregular moon of Saturn that has been used for data recording was 4.8×10^6 km (Ijiraq in September 2014), and the average observation distance was on the order of 14×10^6 km. From this distance, the spatial resolution of the NAC is below 80 km pxl $^{-1}$, too low to resolve the surfaces of the outer moons. The prime observation goal with the NAC was thus to obtain lightcurves to determine rotational periods and other physical parameters, and to improve the orbit ephemeris. During the second half of the mission when most observations took place, the apparent brightness of the irregulars varied between ~ 10 and ~ 37 mag (Phoebe reached up to ~ 5 mag). While the brighter values (compared to Earth-based observers) were a consequence of the smaller distances, the large variation in brightness was a result of the changing phase angles of the irregulars as seen from Cassini, which may in principle have reached any value between 0° and 180° . The large phase-angle range achievable from the Cassini location represented a great advantage for constraining an object's shape from lightcurve inversion, and for the characterization of its photometric properties. Other advantages of the spacecraft-based observations were the absence of Earth-related effects like a day/night cycle (which greatly reduced the period aliasing problem), of the annual opposition cycle, or of weather effects except for storms or rain at the Deep Space Network stations.

From the 38 known irregular moons of Saturn, all 9 progrades and 16 of the 29 retrogrades were successfully observed with Cassini (*DM18*). Thirteen objects were not

observed because of inaccurate ephemeris or because they were too faint. Many moons were targeted repeatedly. As seen from Cassini, almost all the irregular saturnian moons occasionally became brighter than ~ 16.5 mag, a practical limiting magnitude for useful lightcurve studies with the NAC. The apparent brightness at a particular epoch was mainly a function of object size, range, and phase angle. Except for the largest objects, the visibility windows were thus rather limited, and many objects were only observable for a few weeks or months at the frequency of their orbit periods. The competition between the individual irregular moons was indeed so big that not every object that might have been observed during its visibility window has actually been observed.

Measured and derived numbers are compiled in Table 3 and include the following quantities: (1) Rotational periods — these can be determined through proper phasing of repeating lightcurve patterns (e.g., *Harris and Young*, 1989; *Mottola et al.*, 1995); (2) minimum values $(a/b)_{\min}$ for the ratios between the two equatorial diameters of a reference ellipsoid; and (3) the amount of maxima and minima of the measured lightcurves during one rotational cycle. Two maxima and 2 minima ("2-max/2-min") or 3 maxima and 3 minima ("3-max/3-min") was found in almost all lightcurves; some objects "switch" when being observed at different phase angles.

The whole irregular-moon planning and observation process was initiated and performed by one of the authors (T.D.). The use of the Cassini camera was the first use of an interplanetary spacecraft for a systematic photometric survey of a relatively large group of solar system objects.

3.2. Individual Objects

In this section, selected results for each observed moon from the work of *DM18* is presented. A subset of their lightcurves is reproduced in Fig. 2 (again, see Table 3 for a listing of the measured quantities).

(a) Phoebe is covered in section 4, but briefly mentioned here because two Cassini observations were designed to obtain lightcurves at low and high phase angles. These are probably the only lightcurves from Cassini that are not shape-driven, but rather exclusively albedo-driven. Figure 2 shows the Phoebe curve taken at 109° phase angle. The prominent maximum is attributed to bright ice excavated at the rims of large craters Erginus and Jason.

(b) Kiviuq lightcurves taken at low and high phase angle are shown in Fig. 2. The rotational period was determined to 21.97 h ± 0.16 h. The extreme amplitude of 1.7 mag at 31° phase is unique among the observed saturnian irregulars. It indicates that Kiviuq is a very elongated object with an $(a/b)_{\min}$ of at least 2.3, possibly higher. The clear and quite symmetric 2-max/2-min pattern even at high phase is also unique. The lightcurve obtained at 108° phase shows an amplitude of 2.5 mag (or about a factor of 10 in brightness); this is a record among all lightcurves from Cassini measured so far. Kiviuq might even be a contact-binary or

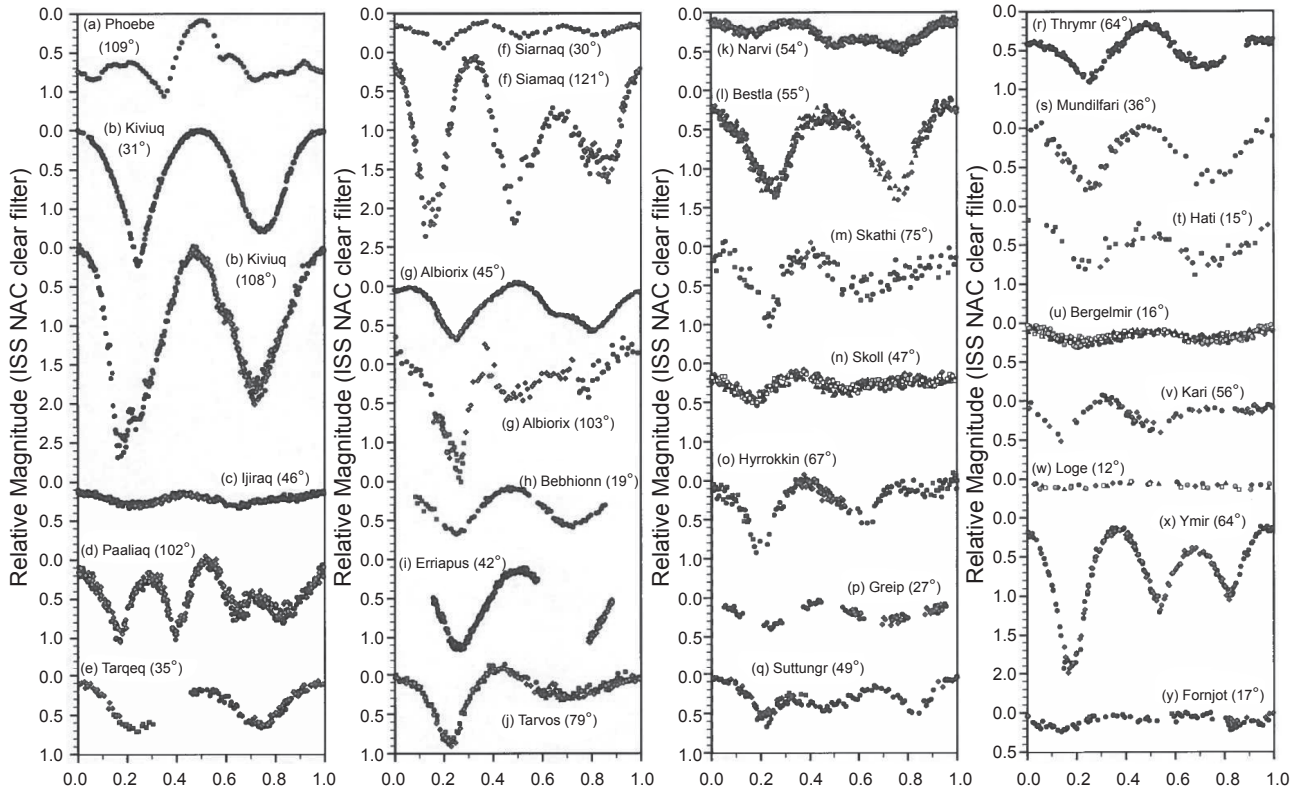


Fig. 2. Lightcurves of 25 irregular moons of Saturn, taken with Cassini ISS NAC at the annotated phase angles. Different symbols indicate different rotational cycles from the same observation or from another observation close in time. Details [moon; observation start MJD (start calendar date, UTC); Cassini orbit (rev = revolution); subspacecraft RA/Dec]:

- Phoebe: 53707.48882 (03 Dec 2005); rev 18; $233^\circ/-18^\circ$
- Kiviuq (31°): 55438.32268 (30 Aug 2010); rev 137; $173^\circ/+27^\circ$
- Kiviuq (108°): 57202.62406 (29 Jun 2015); rev 218; $143^\circ/+40^\circ$
- Ijiraq: 56472.45195 (29 Jun 2013); rev 193; $235^\circ/+30^\circ$
- Paaliaq: 56504.47605 (31 Jul 2013); rev 195; $330^\circ/-24^\circ$
- Tarqeq: 57550.74095 (11 Jun 2016); rev 236; $232^\circ/+10^\circ$
- Siarnaq (30°): 56656.16083 (30 Dec 2013); rev 200; $239^\circ/-42^\circ$
- Siarnaq (121°): 56398.54837 (16 Apr 2013); rev 186; $83^\circ/+60^\circ$
- Albiorix (45°): 55420.18990 (12 Aug 2010); rev 136; $180^\circ/+45^\circ$
- Albiorix (103°): 56455.05408 (12 Jun 2013); rev 192; $138^\circ/-40^\circ$
- Bebhionn: 55322.42646 (06 May 2010); rev 130; $201^\circ/-4^\circ$
- Erriapus: 55229.41932 (02 Feb 2010); rev 125; $142^\circ/+22^\circ$
- Tarvos: 56407.48038 (25 Apr 2013); rev 187; $304^\circ/-47^\circ$
- Narvi: 57396.12153 (09 Jan 2016); rev 230; $284^\circ/-70^\circ$

- Bestla: 56177.41095 (07 Sep 2012); rev 171; $263^\circ/+6^\circ$
- Skathi: 55636.50419 (16 Mar 2011); rev 146; $124^\circ/+31^\circ$
- Skoll: 57440.74498 (22 Feb 2016); rev 232; $210^\circ/+9^\circ$
- Hyrrokkin: 56359.61829 (08 Mar 2013); rev 183; $146^\circ/-11^\circ$
- Grep: 57274.82415 (09 Sep 2015); rev 221; $217^\circ/-10^\circ$
- Suttungr: 57720.50040 (28 Nov 2016); rev 250; $208^\circ/-7^\circ$
- Thrymr: 57013.87652 (22 Dec 2014); rev 210; $170^\circ/-4^\circ$
- Mundilfari: 55995.26586 (09 Mar 2012); rev 162; $167^\circ/-6^\circ$
- Hati: 56351.92441 (28 Feb 2013); rev 182; $222^\circ/+2^\circ$
- Bergelmir: 57278.15338 (13 Sep 2015); rev 221; $227^\circ/-26^\circ$
- Kari: 55498.75138 (29 Oct 2010); rev 140; $144^\circ/+36^\circ$
- Loge: 57074.80992 (21 Feb 2015); rev 212; $228^\circ/-9^\circ$
- Ymir: 56048.42537 (01 May 2012); rev 165; $147^\circ/+22^\circ$
- Fornjot: 56762.10922 (14 Apr 2014); rev 203; $245^\circ/-18^\circ$

binary moon with similarly sized components in a doubly synchronous state; see section 3.3.2 for discussion.

(c) Ijiraq rotates once every 13.03 ± 0.14 h, and all measured data even at high phase and various subspacecraft locations show relatively shallow lightcurves, implying that Ijiraq has a relatively circular equatorial cross-section.

(d) Paaliaq was the first discovery of a prograde irregular saturnian moon. Its name is not taken from the Inuit mythology, but from a fictional Inuit character of a modern novel (Kusugak, 2006). Paaliaq's rotational period is 18.79 ± 0.09 h. Its high-phase lightcurves show a distinct 4-max/4-min pattern, which was not seen in any other lightcurve of the irregulars. Eight relatively clear extrema during one

rotation is very rare throughout the solar system and likely indicative of an unusual shape.

(e) Tarqeeq is the smallest known prograde outer moon and may well be a shard from Siarnaq. From Cassini observations between 2014 and 2017, the rotational period was determined to 76.13 ± 0.04 h. This is by far the longest period of all measured irregular moons, and only a few of the tidally influenced regular moons rotate more slowly. Intriguingly, this period is also very close to the 1:5 resonance of the orbit of Titan (382.690 h), raising the question of tidal alteration of Tarqeeq's rotation. The difference between the Tarqeeq period and one-fifth of the Titan period is only ~ 0.4 h or 0.5% of Tarqeeq's period.

(f) Siarnaq is probably the largest prograde irregular moon of Saturn (*Grav et al.*, 2015) (see also Table 2). The lightcurves show a rather unusual 3-max/3-min pattern with equally spaced but uneven extrema. The amplitudes in high-phase-angle observations are very large (exceeding 2 mag in a 121° phase observation), but shallow at low phases (~0.3 mag in a 30° phase observation; see Fig. 2). Images taken in four different broadband color filters of the NAC at wavelengths between 440 and 860 nm revealed no color variations on the surface. A convex-shape model from seven observations is shown in Fig. 3; Siarnaq resembles a triangular prism in the model. Note that the technique to determine convex-shape models cannot reproduce concavities like craters or other constrictions. The rotational period, which is a sidereal period here, was determined to $10.18785 \text{ h} \pm 0.2 \text{ s}$. The pole axis points toward $\lambda, \beta = 98^\circ/-23^\circ \pm 15^\circ$; this rather low latitude indicates that Siarnaq experiences extreme seasons, somewhat reminiscent of the regular satellites of Uranus. During summer solstice — the most recent on the northern hemisphere approximately occurred in mid-2018 — the Sun might reach the zenith at a surface latitude of 60° to 70° on one hemisphere, while the other remains in a darkness lasting for many years.

(g) Albiorix is the only moon besides Phoebe that became brighter than 10 mag for Cassini. Its lightcurve amplitude at 45° phase is relatively large, indicative of an elongated object. The period was determined to $13.33 \pm 0.03 \text{ h}$. Another observation obtained at a high phase angle of 103° revealed a very different lightcurve shape. While one minimum with an amplitude of 1.5 mag remained prominent, the other disappeared and instead separated into two shallow ones (Fig. 2). The best resolved images have a resolution of 34 km ppxl^{-1} , which is very close to the diameter of this moon. No secondary object was detected in these data.

(h) Bebhionn shows a “nice” 2-max/2-min lightcurve with a quite large amplitude at low phase (Fig. 2), indicative of an elongated object with an $(a/b)_{\min} > 1.4$. From data obtained in 2017, the period was determined to $16.33 \pm 0.03 \text{ h}$.

(i) Erriapus revealed lightcurves with 2-max/2-min patterns and relatively large amplitudes (Fig. 2), indicative of a prolate or possibly contact-binary or binary moon. The rotational period was determined to $28.15 \text{ h} \pm 0.25 \text{ h}$.

(j) Tarvos has a high orbit eccentricity of 0.54, which led to extreme differences in its range to the Cassini spacecraft (6 to $32 \times 10^6 \text{ km}$) at the orbit-period frequency of 2.5 years. Since Tarvos’ periapsis is locked toward the direction of the Sun, the range and phase angle effects canceled each other out for most of the time, resulting in a remarkably constant apparent magnitude seen from Cassini, between ~ 13 and ~ 14.5 during the mission. The rotation period of Tarvos is $10.691 \text{ h} \pm 3 \text{ s}$ and thus quite close to the rotation period of Saturn itself (10.53 to 10.79 h) (*Helled et al.*, 2015). Figure 2 shows a lightcurve from an observation where Tarvos was tracked over more than three rotation cycles at 79° phase. One of the two minima is very pronounced, while the other one is broad and shallow (~0.9 and ~0.4 mag amplitude, respectively).

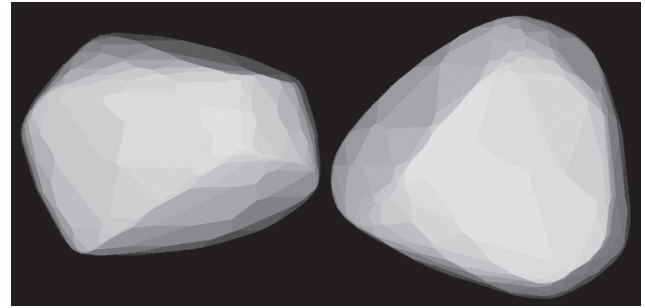


Fig. 3. Convex-shape model of Siarnaq. *Left:* Equatorial view (north up); *right:* north-pole view (rotated around the horizontal axis).

(k) Narvi was observed with Cassini during two observation campaigns, and a rotation period of $10.21 \pm 0.02 \text{ h}$ was found. The lightcurves show a very clear 3-max/3-min pattern including the one-sixth rotational-phase spacing of the extrema seen at Siarnaq and several other moons. A unique feature is that the brightest minimum is brighter than the lowest maximum (Fig. 2).

(l) Bestla is one of the most unusual irregular moons of Saturn because of its extreme orbit elements. The eccentricity of 0.52 is among the highest in the saturnian system, the periapsis distance of $9.7 \times 10^6 \text{ km}$ is among the lowest for retrograde moons, and the orbit inclination of $\sim 145^\circ$ is the lowest of all retrograde moons. Bestla is also the retrograde moon that came closest to outermost regular moon Iapetus during the Cassini mission ($2.3 \times 10^6 \text{ km}$ in November 2003). This is more than three times closer than the closest distance between Iapetus and Phoebe, which was $7.4 \times 10^6 \text{ km}$. Bestla was favorable for Cassini observations every three years. Figure 2 shows a 2-max/2-min lightcurve with a quite large amplitude of 1.1 mag. The sidereal rotation period was determined to $14.6238 \text{ h} \pm 0.4 \text{ s}$. The pole orientation with an ecliptic latitude $\beta = -85^\circ \pm 15^\circ$ is pointing anti-parallel to the normal of the ecliptic, indicating that the rotation is also retrograde.

(m) Skathi has the smallest semimajor axis of any retrograde moon of Saturn except Phoebe, and no other moon is known that shares its orbital elements. From several Cassini observations, its period was determined to $11.10 \pm 0.02 \text{ h}$.

(n) Skoll is another “lonely” moon; it has been observed twice with Cassini. With the second observation from 2016, the period was determined to $7.26 \pm 0.09 \text{ h}$ (Fig. 2). The pattern of the extrema is less pronounced than for Siarnaq, but also contains the “one-sixth spacing” found for the 3-max/3-min lightcurves. For unknown reasons, the 2013 observation could not be fitted well with this period. A secondary frequency from wobble might be the cause, but this is very speculative and cannot be addressed with the available data. The Skoll period thus remains tentative.

(o) Hyrrokkin was observed several times, and its period was determined to $12.76 \pm 0.03 \text{ h}$. Hyrrokkin shows clear

3-max/3-min lightcurves at mid and high phase similar to Ymir and Siarnaq, but with a lower amplitude, only around 1 mag.

(p) Greip was successfully observed in 2015, and the period was determined to 12.75 ± 0.35 h. Since the observation time base of ~ 17.5 h was too short to unambiguously confirm the 2-max/2-min pattern, an ~ 19 -h period is considered less likely, but cannot be ruled out for Greip. The 12.75-h solution is within the errors identical to the Hyrrokkin period. Interestingly, Greip and Hyrrokkin are not just “twins” with respect to the rotational period, but also to their semimajor axes and orbit eccentricities (Table 2), and thus orbit periods, periapsis distances, and apoapsis ranges. Only the orbit inclinations are quite different. The latter makes a joint progenitor less plausible at first glance, but very similar a and e values allow for a scenario where the separation of a progenitor object or binary occurred very close to one of the orbital nodes. Future color observations might indicate if Greip is related to Hyrrokkin or rather to the Suttungr group.

(q) Suttungr was observed in 2011 and 2016, and its rotational period was determined to 7.67 ± 0.02 h. At low phase, the lightcurve shows a 2-max/2-min pattern, while 3-max/3-min were observed at mid phase (Fig. 2).

(r) Thrymr was observed in 2011/2012 and 2014 (Fig. 2), and again in 2017 during the very last Cassini observation of an irregular moon. Because of the long spin period, complete coverage of the rotation could not be achieved during a single Cassini observing request. Assuming the most probable case of a 2-max/2-min lightcurve, the rotation period is 38.79 ± 0.25 h, with the mid-phase lightcurves being reminiscent of Skathi’s or Tarvos’. Thrymr is by far the slowest rotator among the retrograde moons. Somewhat similar to the situation of Hyrrokkin and Greip, the orbital elements a and e , but not i , of Thrymr are close to those of S/2004 S 7, potentially qualifying these two objects as a pair as well. Especially the eccentricities of Thrymr and S/2004 S 7 are much higher than those of the other objects in the Suttungr and Mundilfari families, respectively, of which these two moons might be members as well (Table 2).

(s) Mundilfari was observed by Cassini once over a time span of ~ 9 h at a phase angle of 36° . This was sufficient to determine the rotational period to 6.74 ± 0.08 h. The lightcurve shows a clear 2-max/2-min pattern. Its amplitude of 0.78 mag is substantial, indicating a quite elongated object.

(t) Hati, a small moon with a size of ~ 5 km, might be a member of the Mundilfari cluster. The period of 5.45 ± 0.04 h is the fastest among all 25 measured moons. In the first observation in 2013, Hati was detected near the very edge of a 1×2 mosaic, and the Cassini data helped to improve the orbital elements significantly. The low-phase lightcurve has a relatively high amplitude of 0.55 mag, resulting in a high $(a/b)_{\min}$ of 1.4 to 1.7. Hati’s rotational period is also the fastest reliably known period of all moons in the solar system, including moons of asteroids.

(u) Bergelmir was observed twice with Cassini, and the period was determined to 8.13 ± 0.09 h for a 2-max/2-min

repetitive lightcurve pattern. The lightcurve amplitude of ~ 0.2 mag implies a rather circular equatorial cross-section.

(v) Kari was targeted once with Cassini. With this 16-h observation, the Kari rotational period was determined to 7.70 ± 0.14 h. The lightcurve was taken at 56° phase angle and has an amplitude of ~ 0.5 . The 3-max/3-min pattern with two rather deep minima and one shallow minimum resembles Hyrrokkin’s lightcurve.

(w) Loge is orbiting near the edge of the Saturn system and might be part of a family including Ymir and Fornjot (Fig. 1). Its small size and large distance made this moon very faint for Cassini. An observation in 2015 at 12° phase potentially covered ~ 4.7 rotation cycles, but the SNR of the data was quite low. The amplitude of only ~ 0.07 mag was the shallowest lightcurve measured with Cassini (Fig. 2). The proposed period of 6.9 ± 0.1 h from a 2-max/2-min lightcurve must be considered uncertain.

(x) Ymir has a diameter of ~ 19 km and is, besides Phoebe, the dominant retrograde object in the saturnian system. A relatively large peak-to-peak lightcurve amplitude noted by GB07 from groundbased observations was confirmed with Cassini low-phase data. Ymir is another object that exhibits the 3-max/3-min lightcurve pattern with homogeneously spaced extrema (Fig. 2). The convex-shape model (Denk and Mottola, 2013) reveals a triangular equatorial cross-section very similar to Siarnaq. The pole-axis of Ymir points close to the south-ecliptic pole, indicating a retrograde spin. Ymir’s sidereal period is 11.92220 h ± 0.1 s. Observations through four color filters of the NAC showed no deviation of any color lightcurve from the shape of the clear-filter lightcurve; Ymir is thus uniformly colored on a global scale.

(y) Fornjot is the object with the largest semimajor axis of all known moons of Saturn. It was difficult to observe by Cassini because of its large distance and small size and because of its proximity to the galactic plane, which meant a substantial increase in the number of background stars, during the used opportunities. A period of ~ 6.9 h might work for a 2-max/2-min lightcurve, but the fit is not good. About 9.5 h for 3-max/3-min looks good (Fig. 2), but the lightcurve overlap is very small. This leaves Fornjot as the object with the most uncertain period result among the observed satellites. From the modest lightcurve amplitude, a rather circular equatorial cross-section is expected.

3.3. Patterns and Correlations

Starting from lightcurves and rotational periods obtained for Saturn’s irregular satellites, we searched for statistical patterns; examined the potential of binary and contact-binary objects; looked for potential correlations between the object spins, sizes, and orbit parameters; made bulk-density considerations; and compared the irregular-moon sizes and periods to those of other minor bodies. Orbit dynamical and physical properties are also visualized in an a, i' -diagram that includes information on Saturn distances, orbit tilts, object movement directions, object sizes, spin rates, lightcurve shapes, and potential binarity of the irregulars (Fig. 4).

Herein, the inclination supplemental angle i' is equal to the orbit inclination i for prograde moons, and to $180^\circ - i$ for retrograde satellites.

3.3.1. Lightcurve “end-members.” The number of lightcurve extrema gives a hint on basic shapes of the moons. Satellites Ymir, Siarnaq, Hyrrokkin, Skoll, Kari, Suttung, Narvi, and possibly Fornjot share the 3-max/3-min lightcurve pattern with *six equally spaced* extrema at medium or even low phase angles. For this group of objects, a near-triangular equatorial cross-section is suggested as a proxy for a “convex-shape end-member,” very similar to the model shapes of Siarnaq (Fig. 3) and Ymir. Opposite to this finding, many moons show strict 2-max/2-min lightcurves (Kiviuq, Bestla, Erriapus, Bebhionn, Hati, Mundilfari, Tarqeeq) with *four* extrema quite symmetrically spaced. If this symmetry remains even at high phase angles, a regular ellipsoid is a good first-order shape approximation, and it is suggested that these two model-shape ensembles — ellipsoids and near-triangular prisms — represent some sort of convex-shape end-members among the saturnian moons. Of course, it must be cautioned that the potential variety of shapes is so high that this interpretation has to be considered as first-order only as long as no additional shape information is available, and it also does not include significant concavities or variations between the northern and southern hemispheres. Nevertheless, it gives a rough idea on some object shapes where no shape model is available. The moons with the 3-max/3-min lightcurves at mid or low phase angles are also tagged in

Fig. 4, where they appear to show a random distribution. The only obvious common property is that all have rotation periods faster than 13 h.

3.3.2. Binary candidates. It has repeatedly been proposed and is plausible that irregular moons with very similar orbit parameters (a, e, i) were once a single object that has been separated into two or more pieces by a collision (Fig. 1 and Table 2; see also section 5 for details). In this context and also per se, an interesting question is if there also exist “moons with a moon” that were formed in the course of a collision where the separation conditions of the collisional remnants were such that they remained gravitationally bound to each other, without complete reaccretion into one body. Such “double moons” might exist as binaries with different or equal sizes, or as contact binaries. The outer satellites of the giant planets might be the best places to search for binary configurations among moons because the sizes of their Hill spheres (on the order of ~ 100 to ~ 300 satellite radii; this depends on the moon’s density) are much larger than for the regular satellites (almost all below ~ 20 moon radii).

The review by Margot et al. (2015) about binary asteroids indicates that three distinct types of double objects exist among this group of minor bodies: (1) Large asteroids ($D > 90$ km) with small satellites; (2) small, doubly synchronous binaries with similarly sized components and rather long rotation periods ≥ 13 h; and (3) small (primary-component diameter $D_1 < 11$ km), very rapidly spinning primaries with much smaller secondary components. For types 1 and 3,

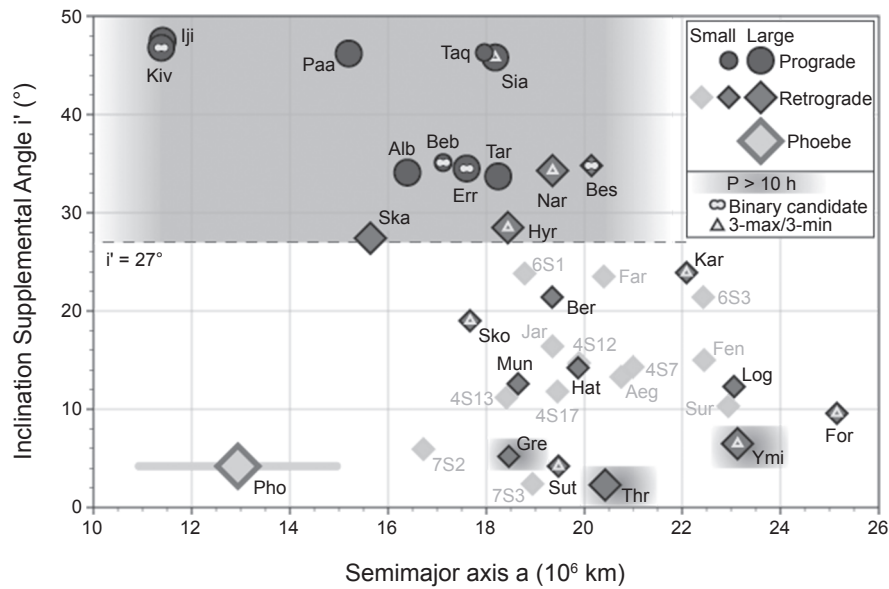


Fig. 4. $a-i'$ plot for 25 irregular moons of Saturn, showing the distributions of object ranges to Saturn (through a), orbit tilts (through inclination supplemental angle i'), orbital senses of motion (pro-/retrograde; through symbols), object sizes (as two equally-sized bins separating into “large” and “small” at absolute magnitude $H \sim 14.4$ mag), and object spin rates (as two bins separated at 2.4 d^{-1} ; the slow rotators are highlighted by a gray background). The light-gray bar at Phoebe indicates its periapsis and apoapsis distance to Saturn. Objects with 3-max/3-min lightcurves at mid or low phase angles as well as binary candidates are marked through insets. The 13 objects not observed by Cassini are included for reference (pale diamonds). They all fall into the categories “small,” “retrograde,” and “low i' ,” and all but one are part of the “farther satellite group.” Their rotational periods are unknown.

only the smaller component rotates synchronously. Binaries of type 1 are usually detected through direct imaging, if their separation allows the components to be resolved. Under particular illumination and viewing geometries, all binaries experience mutual events (occultations and eclipses) that produce signatures in their lightcurves that can be detected from disk-integrated photometry. Such signatures are more easily recognizable in type 3 binaries since the shape-induced brightness variations and those due to mutual events are characterized by different periodicities (rotational and orbital periods, respectively). For this reason, most of the asteroid binaries discovered so far belong to type 3. In type 2 systems, given their full synchronicity, a binary nature is more difficult to demonstrate as the lightcurve signatures due to mutual events are more difficult to distinguish from those due to shape or albedo variations. However, there are lightcurve features that, although not a proof of binarity, can hint at a double nature of a type 2 object (*Lacerda and Jewitt*, 2007; *Margot et al.*, 2015; *Sonnett et al.*, 2015). Such features include high amplitudes, long rotation periods, flat (“plateau-shaped”) extrema, peaked minima, minima of different depth with maxima being equal, highly structured minima, or lightcurve slopes with kinks (e.g., *Lacerda and Jewitt*, 2007). For asteroid binaries, mutual events take place at least every few years. For potential binaries in the saturnian system, “solar-eclipse seasons” occur every ~14–15 years when the orbital nodes of the two bodies line up with the Sun direction. Their durations depend on the rotation-axis orientation as well as the range, the sizes, and the oblatenesses of the components.

Based on these indications, the best candidates for contact-binary or doubly synchronous binary moons from Cassini ISS data are Bestla, Kiviuq, Erriapus, and very possibly Bebhionn. Bestla, with subtle kinks on the lightcurve flanks and a broad plateau-like maximum, and Kiviuq, with its smooth and symmetric 2-max/2-min lightcurves of extreme amplitudes which possess equal maxima but different minima (Fig. 2), are especially promising candidates. Figure 4 shows that these moons all have orbits with a high inclination supplemental angle and are parts of an undoubtedly satellite pair or family. Final proof of binarity, however, requires accurate modeling of the binary system that is capable of exactly reproducing the observed lightcurve features. This effort is undergoing at the time of publication of this chapter.

Figure 5 shows the rotational periods of the primaries P_1 over the diameters of the primaries D_1 for asteroids larger than 1 km. Interestingly, there are large gaps between the three binary types described by *Margot et al.* (2015) that are not necessarily only due to observational bias. Almost all objects of type 3 have a component-diameter ratio $D_2/D_1 \leq 0.5$ (mass ratio <0.2), and none is known showing doubly synchronous rotation. Contrary to this, almost all type 2 asteroids have a component-diameter ratio $D_2/D_1 \geq 0.8$. Adding the saturnian irregular moons to Fig. 5 strengthens the suspicion that Kiviuq, Erriapus, Bestla, or Bebhionn may be doubly synchronous binaries, because they fall in the region of the type 2 objects in the P_1 - D_1 diagram. Contrary to this, most of the other moons occupy regions not typical

for binaries. Thrymr and Tarqeal do fit the slow-period and the 2-max/2-min extrema criteria, but only show moderate lightcurve amplitudes and are thus still possible, but less obvious binary candidates. Paaliaq might also rotate slowly enough, but the shapes of its lightcurves do not suggest a binary system with two separated components, although a contact binary might be a viable option for this moon. Hyrrokkin, Albiorix, and Ijiraq presumably rotate too fast for being binaries, and their lightcurve shapes or amplitudes do not point in this direction as well. Greip’s rotation may also be too fast.

Among the fast rotators of Saturn’s outer moons, no one really falls well within the cluster of the small, fast rotating asteroids with small-mass secondaries (type 3). From Fig. 5, it cannot be ruled out that Hati or another fast rotator possesses a small satellite that was possibly formed through mass shedding, but this cannot be revealed with Cassini data because the time coverage and/or SNR of the available data is insufficient. Therefore, such a search remains a task for a future investigation, possibly with a camera on a future spacecraft mission to Saturn, or through observations of stellar occultations.

3.3.3. Orbit parameters, object sizes, and rotational periods. Among Saturn’s irregular moons, orbital semimajor axes a , orbital senses of motion (through inclinations i), orbit tilts (inclination supplemental angles i'), and object sizes (through absolute magnitudes H) appear to be correlated to some degree. The prograde moons are on average closer to Saturn, on more inclined orbits, and larger than the retrograde objects (Fig. 4). As discussed in section 2.1, the differences for the mean distances between prograde and retrograde moons are partly explained by the modeling result that at large distances, retrograde orbits are more stable than prograde orbits. Furthermore, the ability of Phoebe to collisionally destroy relatively large objects likely explains the lack of moons with smaller semimajor axes and lower tilts, with only some high- i' objects closer to Saturn having been able to escape a collision so far. The orbit-tilt differences between the progrades and the retrogrades might be an origin effect — that the net direction of motion was retrograde for the progenitors of the low- i' objects, but prograde for the high- i' objects, and that the present configuration just reflects the one of the few original progenitors. In case the hypothesis is correct that several dynamical families originate from Phoebe, this might explain the predominance of objects on retrograde orbits. The mainly larger sizes of the progrades are harder to understand; possibly Phoebe cleared a higher amount of low- i' objects’ mass and thus of retrograde objects. Alternatively, the progenitors of the prograde moons might simply have been larger by chance.

The Cassini measurements show that correlations also exist between rotational periods P and the semimajor axes, orbital senses of motion, orbital tilts, and sizes. We divided the group of objects for which rotation periods were available in two samples, comprising objects having semimajor axes smaller and larger than 18.45×10^6 km, respectively. This specific semimajor axis threshold was chosen because

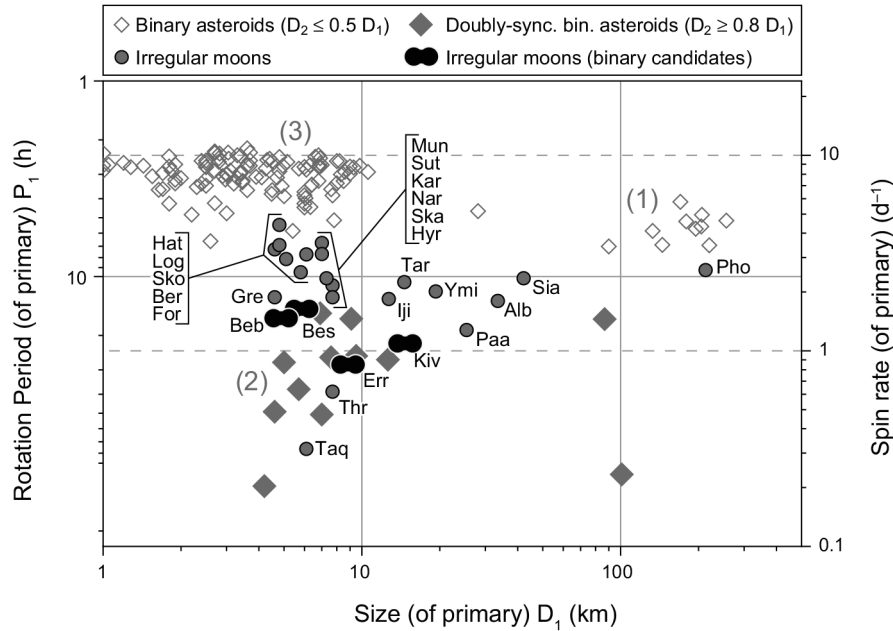


Fig. 5. Primary-component rotation period P_1 over primary-component diameter D_1 for known binary asteroids and for Saturn's irregular moons. For the binary candidates among Saturn's irregulars, the left and right edges of the elongated symbols indicate two diameters as follows: The right edges correspond to the diameters D_1 of the moons in case the moon is no binary ($D_2 = 0$); the left edges show D_1 in the case the object consists of equally-sized binary components ($D_1 = D_2$). The data for the asteroids are from the LCDB (asteroid lightcurve data base) (Warner et al., 2009, accessed on September 5, 2016); the saturnian-moon data are from DM18.

it splits the total sample in two equal-sized groups of 12 members each. (Phoebe was excluded because of its special position with respect to mass and collisional history.) It was found that the median spin rates were 1.8 d^{-1} and 2.7 d^{-1} for the closer and farther satellite group, respectively. A formal Mann-Whitney non-parametric test for median comparison confirmed that the difference is significant at the 95% confidence level. A similar subdivision may also be made for i' and H. For the orbital senses of motion, this may be done as well; only the number of objects in the two samples is now different (9 progrades, 15 retrogrades). In all cases, the rotation periods of the two samples are clearly different from each other. On average, the moons on prograde orbits, at high i', closer to Saturn, and of larger size show longer rotational periods, while most of the smaller, retrograde, low-i', and more-distant objects are the fast rotators. As shown in Fig. 4, there is not even a single object at high i' known in the saturnian system to have a fast spin rate $>2.4 \text{ d}^{-1}$; this includes all prograde moons. Note that all known high-i' moons were measured by Cassini. Opposite to this, rotational periods $>10 \text{ h}$ are rare among the measured lower-i' retrogrades.

No good explanation has been found for these correlations with the periods so far. Since a , i' , the direction of motion, and possibly the size are likely not completely independent, it is plausible that just one or two physical mechanisms may explain all correlations with the spin rate. Tidal dissipation may be considered for the relation between a and P since the despinning timescale is directly proportional to the sixth power of the moon's distance to

the center planet (Peale, 1977). However, the timescale is also inversely proportional to the fifth power of the object size, making tidal despinning as a controlling process for the spin rates of the irregulars unlikely. In fact, despite its large size and closer distance to Saturn, even the despinning of Iapetus is not easy to explain (see, e.g., Castillo-Rogez et al., 2007; Levison et al., 2011).

3.3.4. Bulk densities of fast rotators and potential binaries. The shortest rotation period P_{\min} of an object is limited because it would otherwise break into pieces or at least lose material. P_{\min} depends on the bulk density ρ , the ratio of the equatorial dimensions a/b , and the internal tensile strength; indepth discussions of this problem can be found, e.g., in Davidsson (2001) or Thomas (2009). The fastest known rotators in the saturnian system, Hati and Mundifari, are both rather elongated objects with an a/b of at least 1.4 and possibly up to 1.7 (Hati) or even up to 2.0 (Mundifari). These a/b values correspond to minimum densities of ~ 500 to $\sim 700 \text{ kg m}^{-3}$ (Hati) or ~ 300 to $\sim 500 \text{ kg m}^{-3}$ (Mundifari). For all other irregulars, the minimum bulk densities from rotations are well below 300 kg m^{-3} .

A low density opens up the possibility that the object may be of cometary structure. For example, the density of 67P/Churyumov-Gerasimenko was determined to $533 \pm 6 \text{ kg m}^{-3}$ (Pätzold et al., 2016), and that of 19P/Borrelly to a really lightweight $180\text{--}300 \text{ kg m}^{-3}$ (Davidsson and Gutiérrez, 2004). For an object with $\rho \sim 200 \text{ kg m}^{-3}$, the rotational period cannot be faster than 7.4 h if its shape is an oblate spheroid with negligible tensile strength. For elongated

objects, the critical period increases noticeably. For contact-binaries where the objects are connected near the tips of the single components, a/b (of the equivalent single ellipsoid) mostly exceeds 2 and the minimum rotational period is well above ~ 10 h. For hypothetical binary moons with almost equally sized components (type 2) and with a surface-to-surface minimum distance of one-half the larger component's diameter (for a discussion of this limit, see Margot *et al.*, 2015), the minimum density may be assessed if the orbit period is known and if the component sizes can be reasonably guessed. Depending on the overall configuration, the binary candidates discussed in section 3.3.2 might all be low- ρ objects because they rotate so slowly.

3.3.5. Size and spin compared to other minor bodies.

Comparing average spin rates among different groups of solar system objects is interesting because it might reveal fundamental differences in their compositions or evolutions. The average rotation period for 22 saturnian irregulars of the size range $4 \text{ km} < D < 45 \text{ km}$ (all presented in section 3.2 except Phoebe, Loge, and Fornjot) is 11.4 ± 0.1 h (spin rate $2.10 \pm 0.02 \text{ d}^{-1}$). This is quite slow compared to asteroids at this size range in the inner solar system, but maybe not much different from the Jupiter Trojans or objects beyond Saturn. Figure 6 shows the spin rate over diameter for these objects at the chosen size range. The distributions and average values differ noticeably between the groups.

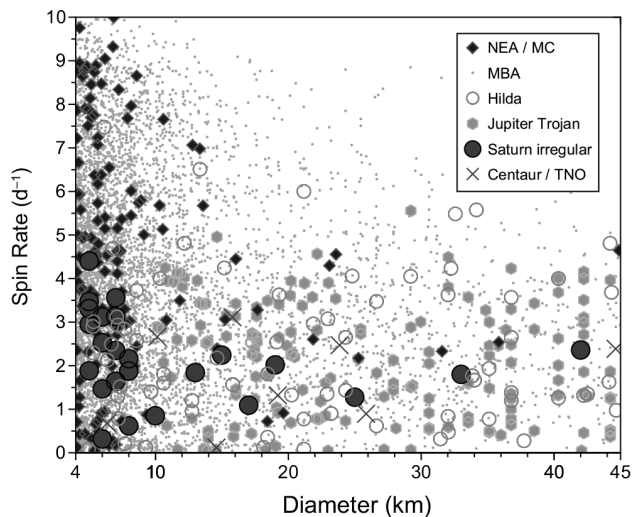


Fig. 6. Object diameters vs. spin rates for various groups of solar-system objects in comparison to the saturnian irregular moons. Shown are objects with sizes between 4 km and 45 km, and with spin rates below 10 d^{-1} . The plotted data, except for the saturnian irregular moons, are from the LCDB (Warner *et al.*, 2009, accessed on September 5, 2016). The average rotational periods for this size range are as follows (in brackets for sizes 10 to 45 km): near-Earth asteroids and Mars crossers: 5.4 h [6.1 h]; main-belt asteroids: 6.4 h [7.0 h]; Hilda asteroids: 10.2 h [10.2 h]; Jupiter Trojans: N/A [11.3 h]; saturnian irregulars: 11.4 h [14.2 h]; Centaurs and TNOs: ~ 13 h.

However, there are different observational biases within these numbers. While the value for the main-belt asteroids should be reliable, the observational cutoff at the small end is ~ 5 km for the Hildas, and ~ 10 km for the Trojans. Small Hildas are thus missing in a statistically significant way, and small Trojans are completely absent in the sample. For the Centaurs/TNOs, only nine objects are in the plot. Even the record of the saturnian moons is incomplete; for the sizes below ~ 6 km ($H \geq 15$ mag), more than half the objects are missing, not counting so-far-undetected moons larger than 4 km.

Nevertheless, the deficit or absence of fast rotators among the outer solar system objects is evident. The figure indicates an increasing upper limit for the spin rate with increasing distance to the Sun. For the Hildas, this boundary appears near ~ 4 to 4.5 h, for the Jupiter Trojans around 5 h. For the saturnian irregulars, as discussed, the fastest rotator (Hati) has a period of ~ 5.5 h, and the larger ones even require > 10 h for one rotation. About one-third of the asteroids of the size range $4 \text{ km} \leq D \leq 45 \text{ km}$ rotate faster than Hati, and more than 60% of the asteroids of the size range $\sim 10 \text{ km} \leq D \leq 45 \text{ km}$ rotate faster than 10 h. Two reasons are proposed for the differences of average spin rates between inner and outer solar system objects. One is the potential efficiency (or lack) of the YORP effect [anisotropic emission of thermal radiation causes a tiny torque to the asteroid (see, e.g., Bottke *et al.*, 2006)], which slowly but steadily changes spin rates of smaller objects in the inner solar system. The other is the supposed lower bulk density of the outer objects, which does not allow them to sustain fast spins as long as they cannot withstand strong tensile stress. Since YORP is not efficient at pushing objects at large heliocentric distances toward the boundary of physical disruption, and because their bulk densities as well as equatorial-diameter ratios should not be homogeneous throughout the populations, and possibly because the number of measured objects might be too low, their spin barriers do not appear as sharp as for the asteroids.

3.3.6. Merging the observations: Thoughts on the physics. The determination of rotational periods for almost two-thirds of Saturn's known irregular moons offered new insights into fundamental properties and poses the question about the physical reasons behind the findings. From the comparison with other small solar system objects (Fig. 6), it appears quite likely that the irregular moons of Saturn, except Phoebe, are rather low-density objects. It is plausible that the real disruption spin barrier for the moons is somewhere between ~ 5 h and ~ 6 h and not near 2.2 h as for the asteroids. The equivalent bulk density of this period range is ~ 300 to $\sim 450 \text{ kg m}^{-3}$ and thus cometary in nature.

Answers to the question about the physical reasons for the found correlations between rotational periods on the one hand and object sizes, semimajor axes, and orbit tilts on the other remain speculative. Due to the lack of straightforward hypotheses, we just offer some thoughts. The first one suggests that the pattern observed and illustrated in Fig. 4 might be due to different physical characteristics of progenitor objects. The destruction and reaccretion processes of the prograde progenitors might have formed rubble-pile

type objects consisting of considerable amounts of water ice with high porosity and, consequently, of a particularly low bulk density. For some reasons, most (~92%) of the current irregular-moon mass outside Phoebe resides in the highly inclined prograde orbits. For the minority of mass farther away from Saturn on lower-tilted retrograde orbits, the different rotational-period properties might be attributed to different physical properties of the progenitors of the different orbit-dynamical families. In particular, the family where Hati is a member might have had a progenitor with a somewhat higher bulk density. This family also contains the second-fastest rotator, Mundilfari, and it would be interesting to see if most of the other six members are also as fast rotators as these two moons are, and if their colors match the neutral color of Mundilfari. A different bulk density and color compared to members of other families may be indicative for a different region of origin in the solar system, somewhat in line with a similar speculation by *GB07* based on the object colors.

The second thought is a corollary to the first one, speculating that many of the retrograde irregular moons might be ejecta from violent impacts on Phoebe. The high-dispersion velocities on the order of 0.5 km s^{-1} do not argue for Phoebe being the origin of some other irregulars, but since Phoebe has survived violent impacts forming craters with sizes up to 100 km, which would easily have pulverized the other moons, debris escaping at much higher speed than from impacts on the smaller moons might in principle be possible. Since Phoebe's density is $\sim 1.6 \text{ g cm}^{-3}$, irregular moons originating from Phoebe should have a significantly higher bulk density than the "cometary" irregulars, even if they are entirely rubble piles. Consequently, the spin barrier for these potential "Phoebe-debris moons" would be at a shorter rotational period than for the "cometary moons." In this scenario, the Mundilfari and the Suttungr families, plus possibly S/2007 S 2 or even Skoll (see Figs. 1 and 4) might result from just a few large impacts on Phoebe, and about half the known retrograde moons might thus have formed this way. The color measurements by *GB07* are consistent and even supportive for such a scenario (Table 3). Although nice, it is incomplete because the fast rotators in the Bergelmir, Kari, and Ymir families are not covered by this explanation unless these were also remnants from Phoebe. It is also generally questionable if ejecta debris from violent impacts that form up to 100-km-sized craters may actually lead to objects with diameters of many kilometers.

The third thought is whether the capture events for the progenitors of the prograde objects might have been different from that of the retrograde moons with respect to the formation regions of the different progenitors. While the objects captured into prograde orbits, by whatever reason, were of low, cometary density, those captured into retrograde orbits had a somewhat higher density. Interesting in this scenario is that only Thrymr and Bestla are the really slow rotators among the numerous retrogrades — the next-slowest retrograde moons, Hyrrokkin and Greip, already have quite fast periods of 12.75 h. Thrymr and Bestla might simply be some

kind of outliers. The situation is exactly opposite for the prograde moons, where all but two objects have rotational periods slower than 13 h.

Finally, the observed distribution of rotational periods vs. sizes, Saturn distances, and inclinations might simply be random. Although we consider this unlikely because the measured differences were found to be significant at a high confidence level, the number of objects available for good statistical considerations is still too small to rule this out. In any case, the Cassini measurements yielded a lot of new information that helps to further characterize these objects and to set further constraints on their formation and evolution.

4. PHOEBE

Phoebe (Fig. 7, Table 4) is the only large irregular satellite of Saturn and the best investigated object of all outer moons in the solar system. It was discovered by William Pickering in 1899 from photographic plates and announced by his brother Edward Pickering (*Pickering*, 1899a,b). Phoebe orbits Saturn at an average distance of ~ 13 million kilometers

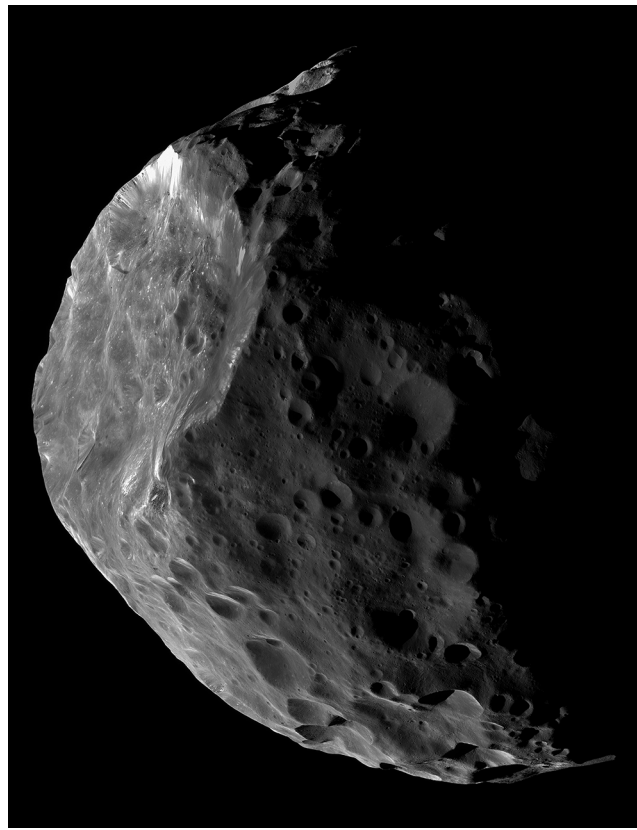


Fig. 7. Global eight-panel mosaic of Phoebe, taken with the Cassini NAC on June 11, 2004, about 0.5 h after closest approach from a distance of $\sim 10,800 \text{ km}$ at a phase angle of $\sim 83^\circ$. North is up. The large $\sim 100\text{-km}$ -sized crater to the left is Jason. The large wall of exposed water ice at the top left of the image belongs to the $\sim 38\text{-km}$ -sized crater Erginus, which is located within Jason. See also Fig. 9 in the chapter by Thomas et al. in this volume for a high-resolution view of Phoebe's surface.

TABLE 4. Phoebe by numbers.

<i>Orbit</i> [*]			
Semimajor axis...	12.948×10^6 km	Eccentricity ...	0.163
Period...	548.02 d	Inclination ...	175.24°
		Orbit direction ...	retrograde
		Mean orbit velocity ...	1.71 km s^{-1}
<i>Body</i> [†]			
Mean radius...	106.4 ± 0.4 km	Ellipsoidal radii ($a \times b \times c$)...	109.3 ± 0.9 km \times 108.4 ± 0.4 km \times 101.8 ± 0.2 km
Volume...	$5.06 \pm 0.20 \times 10^6$ km ³	Mass ...	$829.2 \pm 1.0 \times 10^{16}$ kg
Surface gravity...	0.038 to 0.050 m s ⁻² (~1/200 to ~1/260 g)	Mean density ...	$1642 \pm 18 \text{ kg m}^{-3}$
		Escape velocity ...	89 to 108 m s ⁻¹
<i>Rotation</i> [‡]			
Period...	9.2735 ± 0.0006 h	Spin direction ...	prograde
		J2000 spin-axis ...	RA/Dec = $356.6^\circ \pm 0.3^\circ / +78.0^\circ \pm 0.1^\circ$
<i>Surface</i> [§]			
Geometric albedos:			
B-band ...	0.0855 ± 0.0031	V-band ...	0.0856 ± 0.0023
Bolometric Bond albedo (disk-averaged) ...	0.023 ± 0.007	Range of normal reflectances (Cassini ISS) ...	0.07 to 0.3
Opposition surge (brightness increase from 2° to 0° phase) ...	0.33 ± 0.02 mag		
Spectral slope ...	$-2.5 \pm 0.4\% / 100 \text{ nm}$	Phase integral ...	0.29 ± 0.03
Thermal inertia ...	$\sim 25 \text{ Jm}^{-2}\text{K}^{-1} \text{ s}^{-\frac{1}{2}}$	Macroscopic roughness ...	$33^\circ \pm 3^\circ$
		Temperatures (low-latitude) ...	82 K before dawn to 112 K near subsolar point
<i>Global mosaic and standard map sheet</i> [¶]			
Scale ...	1:1,000,000	Resolution ...	8 ppx deg ⁻¹ or 0.233 km ppx ⁻¹
			Grid system ... Planetocentric lat., west lon.
<i>Interplanetary spacecraft observations</i>			
Voyager 2** ... date:	03/04 Sep 1981	range: 2×10^6 km	spatial resolution: 20 km ppx ⁻¹
Cassini targeted ... date:	10–12 Jun 2004	minimum altitude: 2183 km (to Phoebe center)	no. of images: 552
		best spatial resolution (ISS): 13 m ppx ⁻¹	solar phase angles: 24°–92°
Cassini non-targeted†† ... dates:	06 Aug, 07 Oct 2004; 05 Oct, 06 Nov, 03, 14 Dec 2005; 04 Jan 2006; 07 Jan 2015		
	no. of observations: 8	spatial resol. (ISS): 37–150 km ppx ⁻¹	solar phase angles: 3°–162°

* From JPL solar-system dynamics website (<http://ssd.jpl.nasa.gov>); orbit direction from Pickering (1905).

† Chapter by Thomas et al. (this volume), Castillo-Rogez et al. (2012), Jacobson et al. (2006), Porco et al. (2005).

‡ Bauer et al. (2004), Colvin et al. (1989), Giese et al. (2006).

§ Miller et al. (2011), Buratti et al. (2008), Porco et al. (2005), Thomas (2010), GB07, Flasar et al. (2005).

¶ Roatsch et al. (2006); see also IAU planetary nomenclature (<https://planetarynames.wr.usgs.gov/Page/PHOEBE/target>).

** Thomas et al. (1983).

†† Does not include optical navigation observations.

every 1.5 years in a retrograde orbit, which suggests that it was captured some time in the past (Pollack et al., 1979; Burns, 1986). In 1981, Phoebe was the very first irregular moon from which disk-resolved images were obtained by Voyager 2. The images had shown the satellite to be dark, with relatively small regions that were somewhat brighter (Simonelli et al., 1999), and to have an essentially flat spectrum at visible wavelengths or even a slightly negative spectral slope, i.e., exhibiting a higher reflectance toward the blue and ultraviolet (UV) wavelengths (Tedesco et al., 1989; Simonelli et al., 1999).

On June 11, 2004, during the first and so far only close flyby of an irregular moon, the Cassini-Huygens spacecraft on its way to Saturn orbit insertion came as close as 2070 km to Phoebe's surface to enable high-resolution remote sensing observations and the determination of the satellite's mass and field-and-particle environment. The ISS cameras obtained images at better than 2 km ppx⁻¹ over slightly more than three Phoebe rotations. The highest-resolution ISS images have a pixel scale of 13 m. The mean diameter of Phoebe

was determined to 213 km (Thomas, 2010; Castillo-Rogez et al., 2012). Phoebe's global shape is close to an oblate spheroid, with $a = b$ to within the uncertainties of the data. The calculated volume, combined with the mass determined from radio tracking of the spacecraft, yields a mean density of about 1.64 g cm^{-3} (Thomas, 2010). Phoebe's impact craters range in diameter from the lower limit imposed by the ISS image resolution up to ~ 100 km (crater Jason), which is almost the maximum limit imposed by the size of Phoebe itself. There are more than 130 craters with diameters > 10 km, and about 20 craters are between 25 and 50 km across (Porco et al., 2005).

Bright material on Phoebe appears to be exposed on flat areas and gentle slopes by cratering, and by mass wasting of steep scarps. Bright spots are associated with craters ranging from below the image resolution to ~ 1 km in size. Material excavated by impacts typically comes from depths < 0.1 crater diameters (Gladman et al., 2001); thus, the bright crater deposits represent material from a few meters to ~ 100 m in depth. Bright exposures also occur in landslide debris,

which represents a mixture of materials from a variety of depths. Therefore, the brighter, ice-rich material occurs at both shallow and deeper depths in widespread geographic and geologic settings. However, only a small fraction of craters (<10%) in a limited size range (diameters ≤ 1 km) presently display bright materials. This observation suggests that bright materials either darken or are covered as they age by processes such as (1) infall of dark material from impacts among other small, outer satellites (Melosh, 1989), (2) deposition (regional or global) of debris excavated from elsewhere on Phoebe; (3) sublimation of ice from the bright component, or, possibly, (4) photochemical darkening of impurities in the brighter material.

Cassini ISS found a range of normal albedo from 0.07 to 0.3 (Porco et al., 2005). Local albedo variations on the surface of Phoebe having contrast factors of 2 to 3 as measured by ISS are manifested chiefly as brighter downslope streamers and bright annuli, rays, or irregular bright areas around small craters (Porco et al., 2005). These contrast ratios suggest normal reflectances of ~30% or less, values incompatible with clean ice. Thus, although most of the brighter outcrops are volatile-rich, they are “dirty” (contaminant fraction could still be small) and could evolve to darker lag deposits that mantle Phoebe’s surface through sublimation and thermal degradation processes related to insolation, sputtering, and impact cratering (Porco et al., 2005). Maps of normal reflectance show the existence of two major albedo regimes in the infrared, with gradations between the two regimes and much terrain with substantially higher albedos (Buratti et al., 2008).

Rotational lightcurves derived from the pre-flyby and post-flyby data displayed no substantial variations of whole-disk color with longitude (Porco et al., 2005). The phase curve suggests that Phoebe is overall covered by a mantle of fine particles, resulting from its collisional history or from outgassing (Buratti et al., 2008; Mueller et al., 2008, Miller et al., 2011). The surficial macroscopic roughness of Phoebe was found to be above 30° (Buratti et al., 2008), which is significantly higher than that estimated for many other small bodies ($\sim 20^\circ$) and is consistent with a violent collisional history (Nesvorný et al., 2003; Turrini et al., 2009).

Thermal infrared data of Phoebe acquired by the Composite Infrared Spectrometer (CIRS) onboard the Cassini orbiter (Flasar et al., 2004) during the closest approach phase at a spatial resolution > 8 km showed that temperatures on Phoebe, measured at low latitudes, vary between 82 K and 112 K (Flasar et al., 2005). This diurnal variation yields a thermal inertia of about $25 \text{ J m}^{-2} \text{ K}^{-1} \text{ s}^{-\frac{1}{2}}$ (Flasar et al., 2005), which is comparable to that of many small bodies (asteroids and comets) and is overall indicative of a fine-grained surface regolith.

Based on visible and near-infrared spectra out to 2.4 μm , Owen et al. (2001) identified the bulk composition of Phoebe to be water ice and amorphous carbon. The first identification of non-water-ice volatiles and minerals on Phoebe came from spatially resolved hyperspectral images acquired by the Cassini Visual and Infrared Mapping Spec-

trometer (VIMS), covering the spectral range 0.35–5.1 μm (Brown et al., 2004). These data allowed the identification and mapping of previously detected water ice (Owen et al., 1999), ferrous iron-bearing minerals, bound water, trapped CO₂, trapped H₂, and organics (Clark et al., 2005, 2012). Phoebe’s organic-rich composition is unlike any surface yet observed in the inner solar system, strengthening the possibility that Phoebe is coated by material of cometary or outer solar system origin (Clark et al., 2005).

VIMS mapping indicates that water ice is distributed over most of Phoebe’s observed surface, but generally shows stronger spectral signatures toward the southern polar region (Clark et al., 2005). Spectral parameters measured by VIMS suggest that Phoebe’s CO₂ is native to the body as part of the initial inventory of condensates and now exposed on the surface, strongly mixed with water ice and hydrocarbons (Cruikshank et al., 2010; Filacchione et al., 2010). In medium-resolution VIMS data (4–8 km pxl⁻¹), water ice exposed in the wall of the 38-km crater Erginus (Fig. 7) showed increased abundance of CO₂ and aromatic hydrocarbons, suggesting that these compounds are strongly associated with water ice (Coradini et al., 2008). On the other hand, pixels where CO₂ is depleted showed higher concentrations of non-ice compounds, and vice versa. However, this anti-correlation is not sharp, but rather smooth, with some regions showing an intermediate situation (Coradini et al., 2008). In the highest-resolution data, crater interiors display less exposed ice than the surrounding terrain. The ice-rich layer exposed in crater walls just below Phoebe’s surface and the blue peak seen in the highest-resolution Phoebe spectra imply that the abundance of dark material is low (less than about 2%), and is probably only a surface coating (Clark et al., 2005, 2008).

While Phoebe’s topography, relative to an equipotential surface, is within the range of other small objects and is much higher than that for clearly relaxed objects, the nearly oblate spheroid shape of Phoebe may retain characteristics of an early, relaxed object (Thomas, 2010). Phoebe’s global shape is actually close to that for a hydrostatic-equilibrium spheroid rotating with Phoebe’s spin period (Castillo-Rogez et al., 2012). In particular, the (a-c) value for Phoebe is most compatible with some degree of mass concentration toward the center (Johnson et al., 2009). Phoebe’s low bulk porosity and near-spherical shape suggest that the satellite was not disrupted and subsequently reaccreted. If it were, then the disruption and reaccretion conditions would have had to be very exceptional for Phoebe not to end up as a rubble pile (Castillo-Rogez et al., 2012).

The volatile-rich composition of Phoebe should also reflect, to some extent, the composition of the region where it accreted. One reasonable possibility is that it could have accreted in the volatile-rich outer solar nebula where the Kuiper belt objects (KBOs) originated. Physical properties that Phoebe shares with KBOs include the presence of water ice and an overall low surface albedo (e.g., Brown et al., 1999; Jewitt and Luu, 2004; Pinilla-Alonso et al., 2007). The ratio of water ice to other materials in its interior,

inferred from the average density of the object, might help determine whether Phoebe originated in the solar nebula or in the circum-saturnian disk (Johnson and Lunine, 2005). Mean density is a function of both the sample density and the body's overall porosity. The mean density of Phoebe is higher than the average density of the regular (inner) satellite system of Saturn (excluding Titan), which is $\sim 1300 \text{ kg m}^{-3}$. Based on the average surface composition as derived from VIMS, the plausible range of porosity of Phoebe is from near zero to about 50%. If Phoebe were derived from the same compositional reservoir as Pluto and Triton (whose uncompressed density is $\sim 1900 \text{ kg m}^{-3}$), its present porosity would have to be ~ 0.15 to attain the same material density (Johnson and Lunine, 2005). Even if the porosity of Phoebe were zero, its Cassini-derived density would be 1σ above that of the regular icy saturnian satellites. Therefore, Phoebe appears to be compositionally different from the mid-sized regular satellites of Saturn, ultimately supporting the evidence that it is a captured body (Johnson and Lunine, 2005). Miller et al. (2011) also conclude that Phoebe should originate from the outer solar system. Their photometric study from the ground at very low phase angles indicates that Phoebe's geometric albedo and opposition-surge magnitude are a good match to outer solar system bodies. Regardless of its origin, Phoebe's diverse mix of surface materials probably samples primitive materials in the outer solar system.

Since 1974, it has been postulated that Phoebe may be the source of the low-albedo material coating the leading side of Saturn's moon Iapetus (e.g., Soter, 1974; Mendis and Axford, 1974; Cruikshank et al., 1983; Bell et al., 1985; Burns et al., 1996; Jarvis et al., 2000; Buratti et al., 2005; Verbiscer et al., 2009; Tosi et al., 2010; Tamayo et al., 2011; Cruikshank et al., 2014). Even a single impact event on Phoebe, like the one that originated the medium-sized crater Hylas [diameter 28 km, depth 4.7 km (Giese et al., 2006)], could in principle supply nearly the amount of material needed to darken the leading side of Iapetus (Verbiscer et al., 2009; Tosi et al., 2010). Statistically, a significant fraction of the retrograde dust particles of grain sizes greater than 1 μm impact Iapetus while migrating inward (Tosi et al., 2010).

However, the data indicate that dark material from Phoebe cannot be the only cause of the *albedo dichotomy* of Iapetus as observed today, for four reasons. First, Phoebe's surface is essentially gray and spectrally flat in the visible range and thus substantially different from the reddish color exhibited by the dark material on Iapetus (Owen et al., 2001; Buratti et al., 2002). However, on the basis of Cassini/VIMS data, a higher degree of similarity is found in the near-infrared range between Iapetus and Phoebe, as suggested by the detection of spectral signatures at 2.42 μm , 2.97 μm , and 3.29 μm on both of these bodies (Cruikshank et al., 2008; Clark et al., 2012). Second, there is spectral evidence from Cassini ISS and VIMS suggesting that the dark material on Iapetus has two distinct compositional classes, whose spatial distribution reveals that at least two separate events or mechanisms were responsible for the darkening (Denk et al., 2010; Dalle Ore et al., 2012). Third,

infalling dust would form fuzzy instead of the observed sharp albedo boundaries on Iapetus (Denk et al., 2010). And finally, since dark material from Phoebe almost exclusively hits the leading side of Iapetus, there should be no prominent local dark areas on the trailing side of Iapetus if no other dark material were present. Thus, "other" dark material on Iapetus, presumably intimately mixed in the water ice, should have been a constituent of the surface before the formation of the albedo dichotomy. An (ongoing) deposition of (Phoebe) dust on the leading side of Iapetus was then sufficient to trigger a thermal segregation process, globally redistributing water ice through a self-sustaining process away from low- and mid-latitudes of the leading side toward high latitudes and the trailing side, but no such globally acting process removes water ice from the trailing side or the poles (Spencer and Denk, 2010). The two color classes mentioned above show an unsharp transition near the boundary between the leading and the trailing side of Iapetus in the ISS data (aka near $\sim 0^\circ\text{W}$ and $\sim 180^\circ\text{W}$ longitudes); Denk et al. (2010) dubbed it the *color dichotomy* of Iapetus. This feature is consistent with an origin from Phoebe or the other irregular moons.

An interesting feature related to Phoebe and possibly to the other irregular moons is the so-called *Phoebe ring*, a very faint but huge dust torus around Saturn discovered in Spitzer data at wavelengths of 24 and 70 μm as the result of a dedicated search (Verbiscer et al., 2009). Subsequent observations with the Wide-field Infrared Survey Explorer (WISE) spacecraft at 22 μm showed a radial extension up to $16.3 \times 10^6 \text{ km}$, which is beyond Phoebe's apoapsis distance ($15.1 \times 10^6 \text{ km}$) (Hamilton et al., 2015). The Phoebe ring was also observed through dedicated Cassini ISS observations with the Wide Angle Camera (Tamayo et al., 2014). Kennedy et al. (2011) examined Spitzer data for dust from the non-Phoebe irregulars. From their non-detection, they derive limits for the size distribution of the micrometer-sized dust and conclude that the strength properties of the irregulars should be more porous than expected for asteroids and therefore more akin to comets.

5. ORIGIN OF THE IRREGULAR SATELLITES

The irregular satellites of Saturn have defied conventional origin models for some time. As a population, their orbital properties, size-frequency distributions, and colors are roughly similar to the irregular satellites surrounding Jupiter, Uranus, and Neptune. This means that any scenario that hopes to describe how Saturn's irregular satellites reached their current state might be broadly applicable to those worlds as well. Here we briefly summarize the properties of these populations and refer to the reviews by Sheppard (2006), Jewitt and Haghighipour (2007), and Nicholson et al. (2008) for more details.

Orbits. The irregular satellites fill the stable orbital zones that exist around each giant planet (Carruba et al., 2002; Nesvorný et al., 2003; Shen and Tremaine, 2008). They are located on prograde and retrograde orbits with semimajor

axes values between 0.1 and 0.5 times the distance to their respective planets' Hill sphere. They also have a wide range of eccentricity e and inclination i values ($0.1 < e < 0.7$; $25^\circ < i < 60^\circ$ or $130^\circ < i < 180^\circ$; Nereid: $e = 0.75$, $i = 7^\circ$). Families of fragments with similar orbital properties can also be found, as discussed in previous sections.

Size-frequency distributions (SFDs). The shapes of their cumulative SFDs are unlike any small body population seen anywhere in the solar system (Bottke et al., 2010). The combined prograde and retrograde SFDs at each planet have a cumulative power-law index of $q \sim -1$ for diameters $20 < D < 200$ km. This means that outside the largest objects (e.g., Phoebe at Saturn), they tend to have very little mass. The power-law slopes then change, in some cases dramatically, for $D < 10$ to 30 km. The steepest slopes are seen at Saturn, where $q \sim -3.3$ between $6 < D < 8$ km.

Colors. The irregular satellites have colors that are consistent with dark C-, P-, and D-type asteroids, which are common among the Hilda and Trojan asteroid populations (e.g., Grav et al., 2003, 2004; GB07; Grav and Holman, 2004) as well as in the outer asteroid belt (e.g., Vokrouhlický et al., 2016). These objects are also a good match to the observed dormant comets.

There have been many capture scenarios described in the literature. The various methods of formation could be grouped into three broad categories: drag capture, collision-induced capture, and three-body capture. For drag capture, we have several flavors: capture due to the sudden growth of the gas giant planets, which is often referred to as the "pull-down" capture method (Heppenheimer and Porco, 1977); capture of planetesimals due to the dissipation of their orbital energy via gas drag (Pollack et al., 1979; Astakhov et al., 2003; Ćuk and Burns, 2004; Kortenkamp, 2005); and capture during resonance-crossing events between primary planets at a time when gas drag was still active (Ćuk and Gladman, 2006). Capture by collisions between icy planetesimals is characterized by Colombo and Franklin (1971) and Estrada and Mosqueira (2006). Three-body capture has been considered using three-body exchange reactions between a binary planetesimal and the primary planet (Agnor and Hamilton, 2006; Vokrouhlický et al., 2008; Philpott et al., 2010), and capture in three-body interactions during close encounters between the gas giant planets within the framework of the so-called Nice model (Nesvorný et al., 2007, 2014; and see below).

Reviews of these different scenarios can be found in Jewitt and Haghighipour (2007), Nesvorný et al. (2007), Nicholson et al. (2008), and Vokrouhlický et al. (2008). The arguments they present suggest that nearly all the models above are problematic at some level because they suffer from one or more of the following problems: They are schematic and underdeveloped, they do not really match what is known about planet formation processes and/or planetary physics, their capture efficiency is too low to be viable, they require fine and probably unrealistic timing in terms of gas accretion processes or the turning on/off of gas drag, they cannot reproduce the observed orbits of the irregular satellites, or

they can produce satellites around some but not all gas giants. Moreover, if the outer planets migrate after the capture of the irregular satellites, the satellites themselves will be efficiently removed by the passage of larger planetesimals or planets through the satellite system. This suggests that while different generations of irregular satellites may have existed at different times, the irregular satellites observed today were probably captured in a gas-free environment.

The most successful model at reproducing constraints thus far is from Nesvorný et al. (2007, 2014), with giant planetary migration taking place after the gas disk is gone acting as the conduit for satellite capture. This model takes advantage of the Nice model (Tsiganis et al., 2005; Gomes et al., 2005), a family of solutions where the giant planets started in a different configuration and then experienced migration in response to a dynamical instability. The most successful Nice model simulations are discussed in Nesvorný (2011), Batygin et al. (2012), and Nesvorný and Morbidelli (2012). They assume that the giant planets were once surrounded by a primordial disk of comet-like bodies comprising at least ~ 20 Earth masses. This system was stable for a few tens to a few hundreds of millions of years (e.g., see Bottke and Norman, 2017; Kaib and Chambers, 2016), but eventually became dynamically unstable. This drove Uranus-Neptune into the primordial disk, where their migration through it not only created the observed Kuiper belt and related populations (e.g., Jupiter/Neptune Trojans) (Morbidelli et al., 2005; Nesvorný and Vokrouhlický, 2009; Nesvorný et al., 2013; Gomes and Nesvorný, 2016), but also scattered most of the disk's mass into the giant planet region. A consequence of this migration is that giant planets were encountering one another while surrounded by comet-like objects. This allowed many comets to be captured onto stable giant planet orbits via three-body gravitational interactions (Nesvorný et al., 2007, 2014). Intriguingly, model results show the captured population surviving on stable orbits can reproduce the observed prograde and retrograde irregular satellites remarkably well.

A potential problem with the Nesvorný et al. (2007) model, however, is that it predicts that the irregular satellites should potentially show SFDs similar to those of the Trojan asteroids. Trojan asteroids, having roughly a factor of 5 fewer diameter > 100 -km bodies than the main asteroid belt, have most likely experienced less collisional evolution than the main belt since being captured $\sim 4\text{--}4.5$ G.y. ago. As such, the shape of the Trojan size distribution should be fairly close to the shape it had immediately after capture took place (Wong et al., 2014; Wong and Brown, 2015). An important aspect of irregular satellites, however, is that they were captured into a relatively tiny region of space with short orbital periods around Saturn. This makes high-velocity collisions between irregular satellites unavoidable. Moreover, collision probabilities between typical irregular satellites are 4 orders of magnitude higher than those found among main-belt asteroids (Bottke et al., 2010). An analogy used by Bottke et al. (2010) would be to consider the rate of car crashes occurring along the empty back roads of the

American West (asteroids) to rush-hour traffic in Los Angeles (irregular satellites). Accordingly, their SFDs should undergo rapid and extensive collisional evolution.

Collisional simulations of Bottke *et al.* (2010) show that the prograde and retrograde SFDs quickly grind themselves down from a high-mass into a low-mass state. When low masses are reached, the SFDs may stay in a quasi-collisional steady state for hundreds of millions of years until a stochastic disruption event produces a swarm of new smaller fragments with diameters $D < 1\text{--}7$ km. This fragment trail will then itself slowly grind away on timescales of tens of millions of years until the next stochastic disruption or cratering event on one of the larger remaining satellites produces new ejecta. In this manner, the $D < 7$ km SFDs for both Saturn's prograde and retrograde populations wave up and down again and again over billions of years. The implication is that smaller irregular satellites are mostly fragments of larger bodies, and all have been subjected to numerous impacts since they formed. The orbit-dynamical and compositional families as discussed in sections 2 and 3 (Fig. 1) are an observational support of this one-dimensional model. The prediction is that these populations have lost $\sim 99\%$ of their mass via impacts, making them the most collisionally evolved populations in the solar system. Overall, the model does a good job of explaining the SFD of Saturn's irregular satellites, as well as of those found around the other giant planets. It is also in good agreement with the interpretation of the measured rotational-period distribution vs. object sizes from section 3.3.

A curious yet intriguing prediction for these collisional models concerns the $\sim 99\%$ of the mass lost to comminution over 4 G.y. at each giant planet. The question is what could have happened to all this material. Since the small particles are affected by solar radiation pressure forces and Poynting-Robertson (P-R) drag, they preferentially move inward (Burns *et al.*, 1979). The implication is that the outermost regular satellites of the gas giants could have potentially been blanketed by large amounts of dust produced by a collisional cascade among the irregular satellites, a scenario which in particular the jovian moon Callisto seems to fit (Bottke *et al.*, 2013). For the Saturn system, vast amounts of dust have traveled from Phoebe and the irregular satellites to Iapetus, much visible today on Iapetus' leading hemisphere and possibly hidden beneath upper surface ices. Dust from Phoebe and the irregular satellites also reached Titan. It is speculated that the equatorial longitudinal dune fields that cover a significant fraction of Titan's surface are made of this exogenic material.

6. MISSING INFORMATION AND OUTLOOK

In this chapter, we have briefly summarized the state of knowledge of Saturn's irregular satellites such as orbits, sizes, colors, rotational periods, rough shapes, or bulk-density constraints. In addition, conclusions were discussed such as grouping into dynamical families and possibly pairs similar to the main-belt asteroids; correlations between or-

bital elements, object spin rates, and sizes; then hints of low bulk densities, hints of possible binarity, or the corroboration of the hypothesis that these objects were once formed in other regions of the solar system, later captured and eventually further shredded through collisions over aeons. Research results for Phoebe, in particular some outcome from the unprecedented flyby of Cassini, were presented.

However, despite the advancement in the exploration of the irregular moons of Saturn by Cassini from its vantage point inside the system, many questions remain unanswered and are likely to remain so even when the Cassini dataset will be fully analyzed. For example, we see patterns in the distribution of the lightcurve features and correlations in rotational and dynamical properties (discussed in sections 3.3.3 and 3.3.5; see also Fig. 4) that are not yet explained and that likely relate to the formation process. Furthermore, the capture process for the progenitors of the irregulars is not well understood (section 5). Also, hints for low bulk densities were derived (section 3.3.4), but conclusive measurements with useful error bars do not exist. Another example is the question about the potential existence of binary or contact-binary moons where the Cassini data reach their limits (section 3.3.2).

Although apparently not glamorous science at first glance, probably most important to further increase our understanding of the irregulars is a steady buildup of statistics for both physical and dynamical properties. Discovering more objects and getting more periods and colors (or even spectra) would reveal the described (and probably additional, so far unnoticed) patterns and their (high or low) significance more clearly. As a consequence, boundary conditions for modeling the capture process and the subsequent evolution would become available, which might allow revealing of the history of these objects and thus of a crucial part of the history of the solar system. Ultimately, it is not just the saturnian system that is of interest, but also the irregular-moon systems of Jupiter, Uranus, and Neptune, which are practically unexplored so far.

Due to their faintness and proximity to the bright host planet, most of the irregular moons are challenging targets for physical characterization via Earth-bound observations. As already done for the brightest objects, large telescopes may again be used for targeted observations that do not require vast amounts of telescope time. The situation could further improve in the near future when really giant telescopes, like the Extremely Large Telescope (E-ELT), Thirty Meter Telescope (TMT), or Giant Magellan Telescope (GMT), will be brought into service. These new optical tools might demonstrate their power by barely resolving the largest irregulars and the binary candidates. With these discovery machines on the ground, and in particular with the James Webb Space Telescope (JWST), which is planned to launch to Earth's L₂ Lagrangian point in 2021, spectrophotometry and spectroscopy from the visible to the near-infrared will become possible for numerous irregular satellites. Such studies will enable characterization of the surface composition of these bodies, and will put them in the context of other

populations inhabiting the outer solar system, thereby contributing to addressing the question of their origin.

However, a comprehensive groundbased survey of the rotational properties and convex shapes of the faint irregulars remains difficult due to the large amounts of observing time needed on large telescopes. Amateur astronomers may start to play a role if they can get regular access to telescopes of the 3-m class; adaptive optics, coronographs, and outstanding observation sites would definitely help. Automated surveys like those planned for the Large Synoptic Survey Telescope (LSST) may slowly but steadily sample data, which could eventually provide sparse-sampled lightcurves. Despite the new astrometric catalogs from Gaia, observing stellar occultations to explore possible binary moons is still a big challenge because of the small sizes of the objects and thus very short occultation times — on the order of 1 s or less — and because of the small ground tracks. However, mid-2017 occultation observations of (486958) 2014 MU69 (“Ultima Thule”), the target of the New Horizons spacecraft after the Pluto-Charon flyby, were a comparable challenge, yet they were successful (Buie et al., 2017).

All in all, space missions coming close to the giant planets likely remain key. Even though Cassini was not specifically designed to study irregulars (remember that all but Phoebe were undiscovered when Cassini was launched), and although the spacecraft was more than busy with tasks related to the regular moons (see all other chapters in this book) and other components of the saturnian environment, it made terrific strides in this direction. This achievement was mainly due to two factors: (1) the excellence of the onboard payload, which was not designed to simply “minimum requirements,” but represented the best achievable within the available resources; and (2) the ingenuity and *spirit* of the management, the science, the navigation, and the operations teams, who excelled in designing innovative trajectories and acquisition sequences to seize every possible opportunity to enable new science. The lesson from Cassini should be taken up by every future spacecraft mission: Implement flexibility both in the instrument and in the mission design, in order to be able to readily respond to discoveries that will undoubtedly come. Considering the sum of all advantages and benefits of spacecraft-based research of irregular satellites, we strongly recommend implementing a program to observe these objects in every spacecraft mission to the giant planets.

This final paragraph dares a short look into the far future when humankind might experience crewed spacecraft to the outer solar system. The year is 2118. Curious scientists are eager to explore, impatient tourists are waiting in the wings. Your cargo ship, carrying the future “Kiviuq Base One,” gently approaches its final destination. With the foundation of a station and hotel on this natural stable platform millions of kilometers above the ringed planet lying in your hands, your task to pave the way for the rising era of human expeditions into the wilderness areas of the inner saturnian moons is close to completion. So close to Kiviuq, you head to the main observation deck *just to get the view*

(Fig. 8). Sparkling like a brilliant jewel against the blackness of space, Saturn and its main rings, fully four times larger than the full Moon as seen from Earth, just emerge from behind the small irregular shard and remind you how dreamful, excited, weak, and lonesome a human can feel...



Fig. 8. Saturn comes into view behind Kiviuq while hovering at 400 km altitude during the first-ever landing approach on January 17, 2118, to establish the “Kiviuq Base One” as the gate to the saturnian system for coming scientific and tourist exploration.

Acknowledgments. We thank the reviewers JJ Kavelaars and P. Thomas, as well as editor A. Verbiscer, for their very useful comments and suggestions, which improved the chapter significantly. T.D. thanks the Cassini Imaging team and the Cassini Project at JPL for their impressive support while planning and performing observations with the Cassini-ISS cameras. T.D. gratefully acknowledges the support by the Deutsches Zentrum für Luft- und Raumfahrt (DLR) in Bonn (Germany) (grant no. 50 OH 1503). F.T. gratefully acknowledges the support by the Agenzia Spaziale Italiana (ASI) in Rome (Italy), ASI-INAF grant no. I/2017-10-H.O.

The participation of W.F.B. was supported by NASA's SSERVI program "Institute for the Science of Exploration Targets (ISET)" through institute grant number NNA14AB03A. D.P.H. gratefully acknowledges support from NASA's Cassini Data Analysis Program. T.D. extends a special thanks to G. Neukum (1944–2014), member of the Cassini Imaging team, who allowed him to have access to the Cassini mission and provided the opportunity to help design many observations, especially of the moons of Saturn.

REFERENCES

- Agnor C. B. and Hamilton D. P. (2006) Neptune's capture of its moon Triton in a binary-planet gravitational encounter. *Nature*, **441**, 192–194.
- Astakhov S. A., Burbanks A. D., Wiggins S., and Farrelly D. (2003) Chaos-assisted capture of irregular moons. *Nature*, **423**, 264–267.
- Batygin K., Brown M. E., and Betts H. (2012) Instability-driven dynamical evolution model of a primordially five-planet outer solar system. *Astrophys. J. Lett.*, **744**(1), L3, DOI: 10.1088/2041-8205/744/1/L3.
- Bauer J. M., Buratti B. J., Simonelli D. P., and Owen W. M. (2004) Recovering the rotational light curve of Phoebe. *Astrophys. J.*, **610**, L57–L60, DOI: 10.1086/423131.
- Bauer J. M., Grav T., Buratti B. J., and Hicks M. D. (2006) The phase curve survey of the irregular saturnian satellites: A possible method of physical classification. *Icarus*, **184**, 181–197.
- Bell J. F., Cruikshank D. P., and Gaffey M. J. (1985) The composition and origin of the Iapetus dark material. *Icarus*, **61**, 192–207.
- Blunck J. (2010) *Solar System Moons — Discovery and Mythology*. Springer-Verlag, Berlin. 142 pp. DOI 10.1007/978-3-540-68853-2.
- Bottke W. F. and Norman M. (2017) The late heavy bombardment. *Annu. Rev. Earth Planet. Sci.*, **45**(1), 619–647.
- Bottke W. F., Vokrouhlický D., Rubincam D., and Nesvorný D. (2006) The Yarkovsky and YORP effects: Implications for asteroid dynamics. *Annu. Rev. Earth Planet. Sci.*, **34**, 157–191, DOI: 10.1146/annurev.earth.34.031405.125154.
- Bottke W. F., Nesvorný D., Vokrouhlický D., and Morbidelli A. (2010) The irregular satellites. The most collisionally evolved population in the solar system. *Astron. J.*, **139**, 994–1014.
- Bottke W. F., Vokrouhlický D., Nesvorný D., and Moore J. M. (2013) Black rain: The burial of the Galilean satellites in irregular satellite debris. *Icarus*, **223**, 775–795.
- Brown R. H., Cruikshank D. P., and Pendleton Y. (1999) Water ice on Kuiper belt object 1996 TO₆₆. *Astrophys. J. Lett.*, **519**(1), L101–L104.
- Brown R. H., Baines K. H., Bellucci G., Bibring J.-P., Buratti B. J., Capaccioni F., Cerroni P., Clark R. N., Coradini A., Cruikshank D. P., Drossart P., Formisano V., Jaumann R., Langevin Y., Matson D. L., McCord T. B., Mennella V., Miller E., Nelson R. M., Nicholson P. D., Sicardi B., and Sotin C. (2004) The Cassini Visual and Infrared Mapping Spectrometer (VIMS) investigation. *Space Sci. Rev.*, **115**(1–4), 111–168.
- Buie M. W., Porter S. B., Terrell D., Tamblyn P., Verbiscer A. J., Soto A., Wasserman L. H., Zangari A. M., Skrutskie M. F., Parker A., Young E. F., Benecchi S., Stern S. A., and the New Horizons MU69 Occultation Team (2017) Overview of the strategies and results of the 2017 occultation campaigns involving (486958) 2014 MU69. *AAS/Division for Planetary Sciences Meeting Abstracts*, **49**, #504.01, <http://adsabs.harvard.edu/abs/2017DPS...4950401B>.
- Buratti B. J., Hicks M. D., Tryka K. A., Sittig M. S., and Newburn R. L. (2002) High-resolution 0.33–0.92 μm spectra of Iapetus, Hyperion, Phoebe, Rhea, Dione, and D-type asteroids: How are they related? *Icarus*, **155**, 375–381.
- Buratti B. J., Hicks M. D., and Davies A. (2005) Spectrophotometry of the small satellites of Saturn and their relationship to Iapetus, Phoebe, and Hyperion. *Icarus*, **175**, 490–495.
- Buratti B. J., Soderlund K., Bauer J., Mosher J. A., Hicks M. D., Simonelli D. P., Jaumann R., Clark R. N., Brown R. H., Cruikshank D. P., and Momary T. (2008) Infrared (0.83–5.1 μm) photometry of Phoebe from the Cassini Visual Infrared Mapping Spectrometer. *Icarus*, **193**, 309–322.
- Burns J. A. (1986) The evolution of satellite orbits. In *Satellites* (J. A. Burns and M. S. Matthews, eds.), pp. 117–158. Univ. of Arizona, Tucson.
- Burns J. A., Lamy P. L., and Soter S. (1979) Radiation forces on small particles in the solar system. *Icarus*, **40**, 1–48.
- Burns J. A., Hamilton D. P., Mignard F., and Soter S. (1996) The contamination of Iapetus by Phoebe dust. In *Physics, Chemistry, and Dynamics of Interplanetary Dust* (B. Å. S. Gustafson and M. S. Hanner, eds.), pp. 179–182. ASP Conf. Ser. 104, Astronomical Society of the Pacific, San Francisco.
- Carruba V., Burns J. A., Nicholson P. D., and Gladman B. J. (2002) On the inclination distribution of the jovian irregular satellites. *Icarus*, **158**, 434–449.
- Castillo-Rogez J. C., Matson D. L., Sotin C., Johnson T. V., Lunine J. I., and Thomas P. C. (2007) Iapetus' geophysics: Rotation rate, shape, and equatorial ridge. *Icarus*, **190**, 179–202.
- Castillo-Rogez J. C., Johnson T. V., Thomas P. C., Choukroun M., Matson D. L., and Lunine J. I. (2012) Geophysical evolution of Saturn's satellite Phoebe, a large planetesimal in the outer solar system. *Icarus*, **219**, 86–109, DOI: 10.1016/j.icarus.2012.02.002.
- Clark R. N. and 25 colleagues (2005) Compositional maps of Saturn's moon Phoebe from imaging spectroscopy. *Nature*, **435**, 66–69.
- Clark R. N., Curchin J. M., Jaumann R., Cruikshank D. P., Brown R. H., Hoefen T. M., Stephan K., Moore J. M., Buratti B. J., Baines K. H., Nicholson P. D., and Nelson R. M. (2008) Compositional mapping of Saturn's satellite Dione with Cassini VIMS and implications of dark material in the Saturn system. *Icarus*, **193**(2), 372–386.
- Clark R. N., Cruikshank D. P., Jaumann R., Brown R. H., Stephan K., Dalle Ore C. M., Livo K. E., Pearson N., Curchin J. M., Hoefen T. M., Buratti B. J., Filacchione G., Baines K. H., and Nicholson P. D. (2012) The surface composition of Iapetus: Mapping results from Cassini VIMS. *Icarus*, **218**(2), 831–860.
- Colombo G. and Franklin F. A. (1971) On the formation of the outer satellite groups of Jupiter. *Icarus*, **15**, 186–189.
- Colvin T. R., Davies M. E., Rogers P. G., and Heller J. (1989) *Phoebe: A Preliminary Control Network and Rotational Elements*. NASA STI/Recon Technical Report N-2934-NASA.
- Coradini A., Tosi F., Gavrishi A. I., Capaccioni F., Cerroni P., Filacchione G., Adriani A., Brown R. H., Bellucci G., Formisano V., D'Aversa E., Lunine J. I., Baines K. H., Bibring J.-P., Buratti B. J., Clark R. N., Cruikshank D. P., Combès M., Drossart P., Jaumann R., Langevin Y., Matson D. L., McCord T. B., Mennella V., Nelson R. M., Nicholson P. D., Sicardi B., Sotin C., Hedman M. M., Hansen G. B., Hibbitts C. A., Showalter M., Griffith C., and Strazzulla G. (2008) Identification of spectral units on Phoebe. *Icarus*, **193**(1), 233–251.
- Cruikshank D. P., Bell J. F., Gaffey M. J., Brown R. H., Howell R., Beerman C., and Rognstad M. (1983) The dark side of Iapetus. *Icarus*, **53**, 90–104.
- Cruikshank D. P., Wegryn E., Dalle Ore C. M., Brown R. H., Baines K. H., Bibring J.-P., Buratti B. J., Clark R. N., McCord T. B., Nicholson P. D., Pendleton Y. J., Owen T. C., Filacchione G., and the VIMS Team (2008) Hydrocarbons on Saturn's satellites Iapetus and Phoebe. *Icarus*, **193**, 334–343.
- Cruikshank D. P., Meyer A. W., Brown R. H., Clark R. N., Jaumann R., Stephan K., Hibbitts C. A., Sandford S. A., Mastrapa R. M. E., Filacchione G., Dalle Ore C. M., Nicholson P. D., Buratti B. J., McCord T. B., Nelson R. M., Dalton J. B., Baines K., and Matson D. L. (2010) Carbon dioxide on the satellites of Saturn: Results from the Cassini VIMS investigation and revisions to the VIMS wavelength scale. *Icarus*, **206**(2), 561–572.
- Cruikshank D. P., Dalle Ore C. M., Clark R. N., and Pendleton Y. J. (2014) Aromatic and aliphatic organic materials on Iapetus: Analysis of Cassini VIMS data. *Icarus*, **233**, 306–315.
- Ćuk M. and Burns J. A. (2004) On the secular behavior of irregular satellites. *Astron. J.*, **128**, 2518–2541.
- Ćuk M. and Gladman B. J. (2005) Constraints on the orbital evolution of Triton. *Astrophys. J. Lett.*, **626**, L113–L116.
- Ćuk M. and Gladman B. J. (2006) Irregular satellite capture during planetary resonance passage. *Icarus*, **183**, 362–372.
- Dalle Ore C. M., Cruikshank D. P., and Clark R. N. (2012) Infrared spectroscopic characterization of the low-albedo materials on Iapetus. *Icarus*, **221**(2), 735–743.
- Davidsson B. J. R. (2001) Tidal splitting and rotational breakup of solid biaxial ellipsoids. *Icarus*, **149**, 375–383.
- Davidsson B. J. R. and Gutiérrez P. J. (2004) Estimating the nucleus density of Comet 19P/Borrelly. *Icarus*, **168**, 392–408.
- Denk T. and Mottola S. (2013) Irregular saturnian moon lightcurves

- from Cassini-ISS observations: Update. *AAS/Division for Planetary Sciences Meeting Abstracts*, 45, #406.08. <http://adsabs.harvard.edu/abs/2013DPS...4540608D>.
- Denk T., Neukum G., Roatsch Th., Porco C. C., Burns J. A., Galuba G. G., Schmedemann N., Helfenstein P., Thomas P. C., Wagner R. J., and West R. A. (2010) Iapetus: Unique surface properties and a global color dichotomy from Cassini imaging. *Science*, 327(5964), 435–439, DOI: 10.1126/science.1177088.
- Estrada P. R. and Mosqueira I. (2006) A gas-poor planetesimal capture model for the formation of giant planet satellite systems. *Icarus*, 181, 486–509.
- Filacchione G., Capaccioni F., Clark R. N., Cuzzi J. N., Cruikshank D. P., Coradini A., Cerroni P., Nicholson P. D., McCord T. B., Brown R. H., Buratti B. J., Tosi F., Nelson R. M., Jaumann R., and Stephan K. (2010) Saturn's icy satellites investigated by Cassini-VIMS: II. Results at the end of nominal mission. *Icarus*, 206, 507–523.
- Flasar F. M. and 44 colleagues (2004) Exploring the Saturn system in the thermal infrared: The Composite Infrared Spectrometer. *Space Sci. Rev.*, 115(1–4), 169–297.
- Flasar F. M. and 45 colleagues (2005) Temperatures, winds, and composition in the saturnian system. *Science*, 307, 1247–1251.
- Giese B., Neukum G., Roatsch Th., Denk T., and Porco C. C. (2006) Topographic modeling of Phoebe using Cassini images. *Planet. Space Sci.*, 54, 1156–1166.
- Gladman B., Nicholson P. D., Burns J. A., Kavelaars J. J., Marsden B. G., Williams G. V., and Offutt W. B. (1998) Discovery of two distant irregular moons of Uranus. *Nature*, 392, 897–899.
- Gladman B., Kavelaars J. J., Holman M., Nicholson P. D., Burns J. A., Hergenrother C. W., Petit J.-M., Marsden B. G., Jacobson R., Gray W., and Grav T. (2001) Discovery of 12 satellites of Saturn exhibiting orbital clustering. *Nature*, 412, 163–166.
- Goldreich P. (1966) History of the lunar orbit. *Rev. Geophys. Space Phys.*, 4, 411–439.
- Goldreich P., Murray N., Longaretti P. Y., and Banfield D. (1989) Neptune's story. *Science*, 245, 500–504.
- Gomes R. and Nesvorný D. (2016) Neptune Trojan formation during planetary instability and migration. *Astron. Astrophys.*, 592, A146.
- Gomes R., Levison H. F., Tsiganis K., and Morbidelli A. (2005) Origin of the cataclysmic late heavy bombardment period of the terrestrial planets. *Nature*, 435, 466–469.
- Grav T. and Bauer J. (2007) [GB07] A deeper look at the colors of the saturnian irregular satellites. *Icarus*, 191, 267–285.
- Grav T. and Holman M. J. (2004) Near-infrared photometry of the irregular satellites of Jupiter and Saturn. *Astrophys. J. Lett.*, 605, L141–L144.
- Grav T., Holman M. J., Gladman B. J., and Aksnes K. (2003) Photometric survey of the irregular satellites. *Icarus*, 166, 33–45.
- Grav T., Bauer J. M., Mainzer A. K., Masiero J. R., Nugent C. R., Cutri R. M., Sonnett S., and Kramer E. (2015) NEOWISE: Observations of the irregular satellites of Jupiter and Saturn. *Astrophys. J.*, 809(3), 9 pp.
- Hamilton D. P. (2001) Saturn: Saturated with satellites. *Nature*, 412, 132–133.
- Hamilton D. P., Skrutskie M. F., Verbiscer A. J., and Masci F. J. (2015) Small particles dominate Saturn's Phoebe ring to surprisingly large distances. *Nature*, 522, 185–187.
- Harris A. W. and Young J. W. (1989) Asteroid lightcurve observations from 1979–1981. *Icarus*, 81, 314–364.
- Helled R., Galanti E., and Kaspi Y. (2015) Saturn's fast spin determined from its gravitational field and oblateness. *Nature*, 520, 202–204, DOI: 10.1038/nature14278.
- Hénon M. (1969) Numerical exploration of the restricted problem. V. Hill's Case: Periodic orbits and their stability. *Astron. Astrophys.*, 1, 223–238.
- Heppenheimer T. A. and Porco C. C. (1977) New contributions to the problem of capture. *Icarus*, 30, 385–401.
- Jacobson R. A., Antreasian P. G., Bordi J. J., Criddle K. E., Ionasescu R., Jones J. B., Mackenzie R. A., Pelletier F. J., Owen W. M. Jr., Roth D. C., and Stauch J. R. (2006) The gravitational field of Saturn and the masses of its major satellites. *Astron. J.*, 132, 2520–2526.
- Jacobson R., Brozović M., Gladman B., Alexandersen M., Nicholson P. D., and Veillet C. (2012) Irregular satellites of the outer planets: Orbital uncertainties and astrometric recoveries in 2009–2011. *Astron. J.*, 144(132), 8 pp., DOI: 10.1088/0004-6256/144/5/132.
- Jarvis K. S., Vilas F., Larson S. M., and Gaffey M. J. (2000) Are Hyperion and Phoebe linked to Iapetus? *Icarus*, 146, 125–132.
- Jewitt D. and Haghighipour N. (2007) Irregular satellites of the planets: Products of capture in the early solar system. *Annu. Rev. Astro. Astrophys.*, 45, 261–295.
- Jewitt D. and Luu J. X. (2004) Crystalline water ice on the Kuiper belt object (50000) Quaoar. *Nature*, 432, 731–733.
- Jewitt D., Sheppard S. S., and Kleyna J. (2006) The strangest satellites in the solar system. *Sci. Am.*, 295, 40–47.
- Johnson T. V. and Lunine J. I. (2005) Saturn's moon Phoebe as a captured body from the outer solar system. *Nature*, 435, 69–71.
- Johnson T. V., Castillo-Rogez J. C., Matson D. L., and Thomas P. C. (2009) Phoebe's shape: Possible constraints on internal structure and origin. In *Lunar and Planetary Science XL*, Abstract #2334. Lunar and Planetary Institute, Houston.
- Johnston W. R. (2018) Asteroids with Satellites. <http://www.johnstonsarchive.net/astro/asteroidmoons.html> [accessed April 29, 2018].
- Kaib N. A. and Chambers J. E. (2016) The fragility of the terrestrial planets during a giant-planet instability. *Mon. Not. R. Astron. Soc.*, 455, 3561–3569.
- Kennedy G. M., Wyatt M. C., Su K. Y. L., and Stansberry J. A. (2011) Searching for Saturn's dust swarm: Limits on the size distribution of irregular satellites from km to micron sizes. *Mon. Not. R. Astron. Soc.*, 417, 2281–2287.
- Kortenkamp S. J. (2005) An efficient, low-velocity, resonant mechanism for capture of satellites by a protoplanet. *Icarus*, 175, 409–418.
- Kruse S., Klavetter J. J., and Dunham E. W. (1986) Photometry of Phoebe. *Icarus*, 68, 167–175.
- Kusugak M. (2006) *The Curse of the Shaman*. Harper Trophy Canada, Toronto. 158 pp.
- Lacerda P. and Jewitt D. C. (2007) Densities of solar system objects from their rotational lightcurves. *Astron. J.*, 133, 1393–1408.
- Levison H. F., Walsh K. J., Barr A. C., and Dones L. (2011) Ridge formation and de-spinning of Iapetus via an impact-generated satellite. *Icarus*, 214, 773–778.
- Margot J.-L., Pravec P., Taylor P., Carry B., and Jacobson S. A. (2015) Asteroid systems: Binaries, triples, and pairs. In *Asteroids IV* (P. Michel et al., eds.), pp. 355–374. Univ. of Arizona, Tucson, DOI: 10.2458/azu_uapress_9780816532131-ch019.
- Melosh H. J. (1989) *Impact Cratering: A Geologic Process*. Oxford, New York. 253 pp.
- Mendis D. A. and Axford W. I. (1974) Satellites and magnetospheres of the outer planets. *Annu. Rev. Earth Planet. Sci.*, 2, 419–474.
- Miller C. A., Verbiscer A. J., Chanover N. J., Holtzman J. A., and Helfenstein P. (2011) Comparing Phoebe's 2005 opposition surge in four visible light filters. *Icarus*, 212, 819–834.
- Morbidelli A., Levison H. F., Tsiganis K., and Gomes R. (2005) Chaotic capture of Jupiter's Trojan asteroids in the early solar system. *Nature*, 435, 462–465.
- Mottola S., De Angelis G., Di Martino M., Erikson A., Hahn G., and Neukum G. (1995) The Near-Earth Objects Follow-Up Program: First results. *Icarus*, 117, 62–70.
- Mueller M., Grav T., Trilling D., Stansberry J., and Sykes M. (2008) Size and albedo of irregular saturnian satellites from Spitzer observations. *AAS/Division for Planetary Sciences Meeting Abstracts*, 40, #61.08, <http://adsabs.harvard.edu/abs/2008DPS...40.6108M>.
- Nesvorný D. (2011) Young solar system's fifth giant planet? *Astrophys. J. Lett.*, 742, L22.
- Nesvorný D. and Morbidelli A. (2012) Statistical study of the early solar system's instability with four, five, and six giant planets. *Astron. J.*, 144, 117.
- Nesvorný D. and Vokrouhlický D. (2009) Chaotic capture of Neptune trojans. *Astron. J.*, 137(6), 5003–5011.
- Nesvorný D., Alvarez J. L. A., Dones L., and Levison H. F. (2003) Orbital and collisional evolution of the irregular satellites. *Astron. J.*, 126, 398–429.
- Nesvorný D., Vokrouhlický D., and Morbidelli A. (2007) Capture of irregular satellites during planetary encounters. *Astron. J.*, 133, 1962–1976.
- Nesvorný D., Vokrouhlický D., and Morbidelli A. (2013) Capture of trojans by jumping Jupiter. *Astrophys. J.*, 768(1), DOI: 10.1088/0004-637X/768/1/45.
- Nesvorný D., Vokrouhlický D., and Deienno R. (2014) Capture of irregular satellites at Jupiter. *Astrophys. J.*, 784, 22.
- Nicholson P. D., Čuk M., Sheppard S. S., Nesvorný D., and Johnson

- T. V. (2008) Irregular satellites of the giant planets. In *The Solar System Beyond Neptune* (M. A. Barucci et al., eds.), pp. 411–424. Univ. of Arizona, Tucson.
- Nogueira E., Brasser R., and Gomes R. (2011) Reassessing the origin of Triton. *Icarus*, *214*, 113–130.
- Owen T. C., Cruikshank D. P., Dalle Ore C. M., Geballe T. R., Roush T. L., and de Bergh C. (1999) Detection of water ice on Saturn's satellite Phoebe. *Icarus*, *139*(2), 379–382.
- Owen T. C., Cruikshank D. P., Dalle Ore C. M., Geballe T. R., Roush T. L., de Bergh C., Meier R., Pendleton Y. J., and Khare B. N. (2001) Decoding the domino: The dark side of Iapetus. *Icarus*, *149*, 160–172.
- Pätzold M., Andert T., Hahn M., Asmar S. W., Barriot J.-P., Bird M. K., Häusler B., Peter K., Tellmann S., Grün E., Weissman P. R., Sierks H., Jorda L., Gaskell R., Preusker F., and Scholten F. (2016) A homogeneous nucleus for Comet 67P/Churyumov-Gerasimenko from its gravity field. *Nature*, *530*, 63–65, DOI: 10.1038/nature16535.
- Peale S. J. (1977) Rotation histories of the natural satellites. In *Planetary Satellites* (J. A. Burns, ed.), pp. 87–112. Univ. of Arizona, Tucson.
- Pecaut M. J. and Mamajek E. E. (2013) Intrinsic colors, temperatures, and bolometric corrections of pre-main-sequence stars. *Astrophys. J. Suppl.*, *208*(9), 22 pp.
- Philpott C., Hamilton D. P., and Agnor C. B. (2010) Three-body capture of irregular satellites: Application to Jupiter. *Icarus*, *208*, 824–836.
- Pickering E. C. (1899a) A new satellite of Saturn. *Harvard College Observatory Bulletin*, No. 49, March 17, 1899.
- Pickering E. C. (1899b) A new satellite of Saturn. *Harvard College Observatory Circular*, No. 43, 3 pp. (Also reprinted in *Astronomische Nachrichten*, *356*2, 189–192; *Astrophys. J.*, *9*(4), 274–276; *Nature*, *60*(1540), 21–22; *Pop. Astron.*, *7*, 233–235.)
- Pickering W. H. (1905) The ninth satellite of Saturn. *Ann. Harvard College Observatory*, *53*(3), 45–73.
- Pinilla-Alonso N., Licandro J., Gil-Hutton R., and Brunetto R. (2007) The water ice rich surface of (145453) 2005 RR₄₃: A case for a carbon-depleted population of TNOs?. *Astron. Astrophys.*, *468*, L25–L28.
- Pollack J. B., Burns J. A., and Tauber M. E. (1979) Gas drag in primordial circumplanetary envelopes: A mechanism for satellite capture. *Icarus*, *37*, 587–611.
- Porco C. C., West R. A., Squyres S. W., McEwen A. S., Thomas P. C., Murray C. D., Del Genio A., Ingersoll A. P., Johnson T. V., Neukum G., Veverka J., Dones L., Brahic A., Burns J. A., Haemmerle V., Knowles B., Dawson D., Roatsch Th., Beurle K., and Owen W. (2004) Cassini imaging science: Instrument characteristics and capabilities and anticipated scientific investigations at Saturn. *Space Sci. Rev.*, *115*, 363–497, DOI: 10.1007/s11214-004-1456-7.
- Porco C. C., Baker E., Barbara J., Beurle K., Brahic A., Burns J. A., Charnoz S., Cooper N., Dawson D. D., Del Genio A. D., Denk T., Dones L., Dyudina U., Evans M. W., Giese B., Grazier K., Helfenstein P., Ingersoll A. P., Jacobson R. A., Johnson T. V., McEwen A. S., Murray C. D., Neukum G., Owen W. M., Perry J., Roatsch T., Spitali J., Squyres S. W., Thomas P. C., Tiscareno M., Turtle E. P., Vasavada A. R., Veverka J., Wagner R., and West R. (2005) Cassini imaging science: Initial results on Phoebe and Iapetus. *Science*, *307*, 1237–1242.
- Roatsch Th., Wählisch M., Scholten F., Hoffmeister A., Matz K.-D., Denk T., Neukum G., Thomas P. C., Helfenstein P., and Porco C. C. (2006) Mapping of the icy saturnian satellites: First results from Cassini-ISS. *Planet. Space Sci.*, *54*, 1137–1145.
- Shen Y. and Tremaine S. (2008) Stability of the distant satellites of the giant planets in the solar system. *Astron. J.*, *136*, 2453–2467.
- Sheppard S. S. (2006) Outer irregular satellites of the planets and their relationship with asteroids, comets and Kuiper belt objects. In *Asteroids, Comets, Meteors (ACM)* (D. Lazzaro et al., eds.), pp. 319–334. IAU Symp. No. 229, Cambridge Univ., Cambridge.
- Simonelli D. P., Kay J., Adinolfi D., Veverka J., Thomas P. C., and Helfenstein P. (1999) Phoebe: Albedo map and photometric properties. *Icarus*, *138*, 249–258.
- Sonnett S., Mainzer A., Grav T., Masiero J., and Bauer J. (2015) Binary candidates in the Trojan and Hilda populations from NEOWISE light curves. *Astrophys. J.*, *799*, 191, 20 pp.
- Soter S. (1974) Brightness of Iapetus. Paper presented at IAU Colloquium 28, Cornell University, Ithaca.
- Spencer J. R. and Denk T. (2010) Formation of Iapetus's extreme albedo dichotomy by exogenically-triggered thermal migration of water ice. *Science*, *327*(5964), 432–435, DOI: 10.1126/science.1177132.
- Tamayo D., Burns J. A., Hamilton D. P., and Hedman M. M. (2011) Finding the trigger to Iapetus' odd global albedo pattern: Dynamics of dust from Saturn's irregular satellites. *Icarus*, *215*, 260–278.
- Tamayo D., Hedman M. M., and Burns J. A. (2014) First observations of the Phoebe ring in optical light. *Icarus*, *233*, 1–8.
- Tedesco E. F., Williams J. G., Matson D. L., Weeder G. J., Gradie J. C., and Lebofsky L. A. (1989) A three-parameter asteroid taxonomy. *Astron. J.*, *97*, 580–606.
- Thomas N. (2009) The nuclei of Jupiter family comets: A critical review of our present knowledge. *Planet. Space Sci.*, *57*, 1106–1117, DOI: 10.1016/j.pss.2009.03.006.
- Thomas P. C. (2010) Sizes, shapes, and derived properties of the saturnian satellites after the Cassini nominal mission. *Icarus*, *208*, 395–401, DOI: 10.1016/j.icarus.2010.01.025.
- Thomas P. C., Veverka J., Davies M. E., Morrison D., and Johnson T. V. (1983) Phoebe: Voyager 2 observations. *J. Geophys. Res.*, *88*, 8736–8742.
- Tosi F., Turrini D., Coradini A., Filacchione G., and the VIMS Team (2010) Probing the origin of the dark material on Iapetus. *Mon. Not. R. Astron. Soc.*, *403*(3), 1113–1130.
- Tremaine S., Touma J., and Namouni F. (2009) Satellite dynamics on the Laplace surface. *Astron. J.*, *137*, 3706–3717.
- Tsiganis K., Gomes R., Morbidelli A., and Levison H. F. (2005) Origin of the orbital architecture of the giant planets of the solar system. *Nature*, *435*, 459–461.
- Turrini D., Mazari F., and Beust H. (2008) A new perspective on the irregular satellites of Saturn — I. Dynamical and collisional history. *Mon. Not. R. Astron. Soc.*, *391*, 1029–1051.
- Turrini D., Mazari F., and Tosi F. (2009) A new perspective on the irregular satellites of Saturn — II. Dynamical and physical origin. *Mon. Not. R. Astron. Soc.*, *392*, 455–474.
- Verbiscer A. J., Skrutskie M. F., and Hamilton D. P. (2009) Saturn's largest ring. *Nature*, *461*, 1098–1100, DOI: 10.1038/nature08515.
- Vokrouhlický D., Nesvorný D., and Levison H. F. (2008) Irregular satellite capture by exchange reactions. *Astron. J.*, *136*, 1463–1476.
- Vokrouhlický D., Bottke W. F., and Nesvorný D. (2016) Capture of trans-neptunian planetesimals in the main asteroid belt. *Astron. J.*, *152*, 39.
- Warner B. D., Harris A. W., and Pravec P. (2009) The asteroid lightcurve database. *Icarus*, *202*, 134–146, DOI: 10.1016/j.icarus.2009.02.003.
- Wong I. and Brown M. E. (2015) The color-magnitude distribution of small Jupiter Trojans. *Astron. J.*, *150*, 174.
- Wong I. and Brown M. E. (2016) A hypothesis for the color bimodality of Jupiter Trojans. *Astron. J.*, *152*, 90.
- Wong I., Brown M. E., and Emery J. P. (2014) The differing magnitude distributions of the two Jupiter Trojan color populations. *Astron. J.*, *148*, 112.